FACULDADE DE ENGENHARIA DA UNIVERSIDADE DO PORTO

Dynamics and Attitute Estimation and Control of a Spacecraft System

Diana Sofia Gaspar Almeida

Mestrado Integrado em Engenharia Eletrotécnica e de Computadores

Supervisor: Professor Doutor Antonio Pedro Rodrigues Aguiar

July 26, 2018

Resumo

Esta dissertação tem como principal objectivo a estimação e controlo da dinâmica da atitude de um satélite.

Ao longo da dissertação é apresentada a análise e implementação em simulação de um sistema do satélite. O sistema é constituído pelos modelos funcionais ambiente, dinâmica, equipamento (sensores e atuadores) e controlador. No modelo do ambiente, investiga-se o cálculo da órbita do satélite usando as leis de Newton e de Kepler. Também foi realizada uma comparação entre as duas leis de forma a distinguir as diferenças entre elas. Na parte da dinâmica e dos sensores e actuadores é feito um estudo à representação da cinemática do satélite utilizando quaterniões e à dinâmica do satélite. Também é realizado o estudo da contribuição para a dinâmica do satélite do sub-sistema dos actuadores. Os capítulos seguintes são dedicados aos métodos para a estimação da atitude do satélite e em que condições são utilizados os diferentes métodos de estimação. De seguida também é feito o estudo do controlador do satélite.

Para finalizar, a dissertação também dedica especial atenção ao lixo espacial e os satélites que já não estão em funcionamento. O número destes satélites é cada vez maior e existe a necessidade de implementar novas medidas de forma a evitar colisões com outros satélites ou a entrada de detritos na atmosfera na Terra. Nesta dissertação faz-se um estudo preliminar, análise e implementação da navegação e o controlo do "e.Deorbit" desde da fase em que se sabe qual é o alvo até à sua captura.

Palavras-Chave: dinâmica de um satélite, controlo de atitude, estimação, rendezvous de satélites, satélite.

Abstract

The main goal of this dissertation is the dynamics modeling, estimation and attitude control of a satellite.

Throughout the dissertation is presented the implementation and analysis of a general system of a satellite. The system consists on environment, dynamics, equipment (sensors and actuators) and controller models. In the environment functional system, it is demonstrated how the satellite orbit is calculated using the laws of Newton and Kepler. A comparison between the two laws in order to distinguish the differences between them are also presented. Next, the dynamics, sensors and actuators of a satellite are investigated. In particular, the use of quaternions are investigated to represent the attitude of the satellite. We also made a study about the contribution made by the actuators subsystem on the satellite's dynamic. The next chapters are dedicated to estimation and satellite attitude control.

Whereas space debris and satellites that are obsolete are growing more and more there is a need to implement new measures to avoid accidents, such as collisions with other satellites or the entry of debris on Earth's atmosphere. In this dissertation we also study, analyse and implement the guidance navigation and control of "e.Deorbit" from the phase that it knows what is its target until its capture.

Keywords: Satellite dynamics, estimation, spacecraft, space rendezvous, attitude control

Acknowledgments

Firstly I would like to express my sincere thanks to my supervisor, Prof./Dr. António Pedro Aguiar, for his continuous support and knowledge.

I would like to thank my brother Sérgio for all the encouragement given and the kind words on the right moments, my mother Deolinda, grandmother, Kelly and Maia for all their support.

Diana Sofia Gaspar Almeida

"Don't let what you cannot do
interfere with what you can do"

John Wooden

Contents

List of Figures

List of Tables

Glossary

ADCS	Attitude determination and control subsystem
CESS	Coarse Earth and Sun Sensors
C-W	Clohessy-Wiltshire
PD control	Proportional-Derivative controller
RODC	Rendezvous orbital dynamics and control
SISO	Single-input-single-output
SSO	Sun-synchronous orbit
STR	Star Tracker
ODE	Ordinary differential equation
ORION	On-orbit servicing and navigation
OSS	On-orbit servicing of satellites

Chapter 1

Introduction

1.1 Context

We depend directly or indirectly on satellites to communicate, entertainment, information and so much more.

Since the beginning of the space exploration, satellites have been good tools to study solar system and other systems. Systems interact with the environment and with other systems. Sometimes, we can ignore those interactions between systems when testing software and integrated electronic equipment. However, when we deal with control systems, open loop testing is inadequate because only hardly could one effectively and efficiently define an adequate combination of inputs and expected outputs. Therefore, some systems require closed loop testing and that implies to simulate external systems, the system under test interacts with the environment and systems dynamics.

The satellite's sun-synchronous orbits travels from north to the south poles while the Earth turns and the satellite pass at the same time every day through the same region of the Earth (see Figure 1.1). Those orbits are very useful for weather satellites, climate studies, imaging and to control human activity.

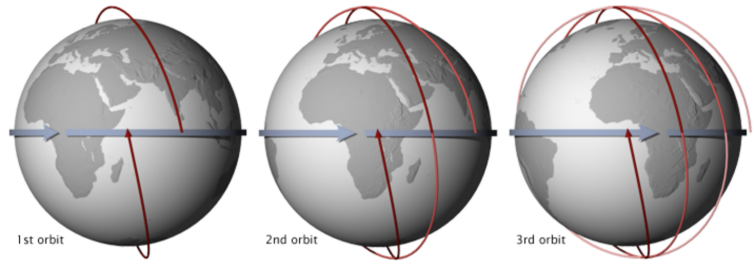

Figure 1.1: Sun-synchronous orbit.
Source: [55]

Unfortunately, the satellites have a limited life time and when they are inoperative many continue to orbit around the Earth. When obsolete satellites do not decay, they are consequently just getting in the way of another satellite. Over the years debris has accumulated around the Earth. Now, ESA has been studying new measures to remove the debris and promote green technologies.

1.2 Goals

The main goal of this Dissertation is to analyse and to implement a Sun-synchronous satellite system, see figure 1.2.

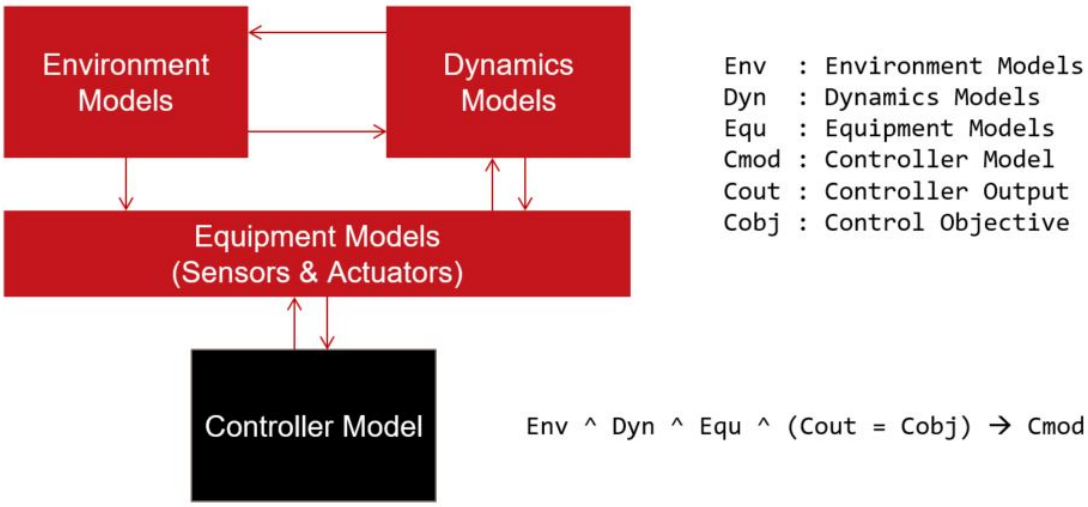

Figure 1.2: Spacecraft system.

Particular points that will be addressed in simulation include:

- implementation and simulation of the spacecraft relative positions of the Earth with Newton's Laws;
- implementation the actuators of a spacecraft;
- implementation kinematics and dynamics of a spacecraft;
- implementation and simulation of the attitude estimation;
- implementation and simulation the attitude controller with actuator;

1.3 Motivation

Satellites are more important to our lives than we may think. With the study of satellites we can improve our life quality. For example, without satellites we could not have wireless communications like cellphones nor smartphones with internet connection nor we could watch live TV from the other side of the Earth.

Nowadays many people in the morning use their mobile phone to get updated on the news and to check those little things are already part of our routine that we do without even realise how much technology we need just to know the weather. For these reasons and many other, it is very important to study satellites and their orbits.

However, there are many satellites that are obsolete and now they are just debris. To continue the space exploration we need to implement new measures and adopt to green technologies. We also need to apply this measures if we want to continue to live as we are living nowadays.

1.4 Organization of the Dissertation

This Dissertation is divided into eight chapters. The first chapter is a contextualisation of Dissertation, objectives and motivation. We then provide an introduction to Copernicus programme and bibliographical review of some concepts. In the third chapter we present a brief survey of orbit dynamics and the difference between the Kepler's Laws and Newton's Universal Law of Gravitation. The fourth chapter is dedicated to the kinematics and dynamics of a spacecraft. Also in fourth chapter we present the actuators implementation in a spacecraft. The fifth chapter is dedicated to the attitude estimation of a spacecraft using the filter estimation. Then, in the next chapter we present the attitude control of a spacecraft. The seventh chapter is dedicated to the space rendezvous. Finally, the eighth chapter describes the main conclusions and future work.

Chapter 2

Literature Review

This chapter begins with a brief introduction of Copernicus programme, theory of sun-synchronous orbit, clean space and 5G-satellites.

2.1 Copernicus programme

This dissertation is inspired by the Copernicus program. Whose main goal is to observe the environment, collect and analyze data and provide equipment to improve the state of planet Earth. There is a set of Sentinel satellites that are part of this program. Each Sentinel satellite has a specific role in monitoring changes in soil, oceans and atmosphere. So far Sentinel-1, Sentinel-2, Sentinel-3 Sentinel-4, Sentinel-5 are in orbit. And Sentinel-6 and EarthCARE are still in construction phase.

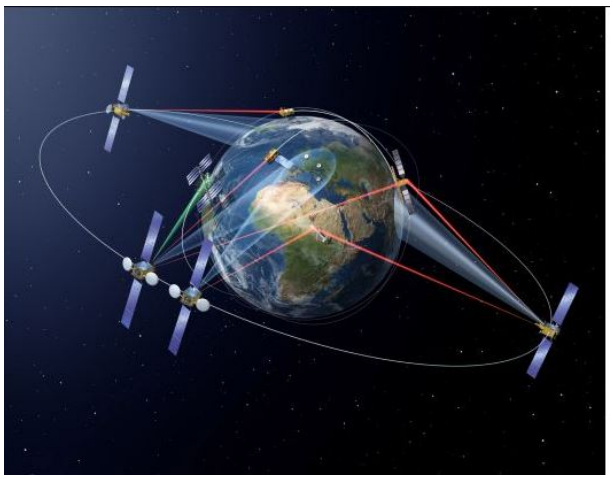

Figure 2.1: Copernicus programme
Source: [56]

As shown below each Sentinel and EarthCARE satellites mission has a specific mission:

- **Sentinel-1**: land monitoring changes by collecting data on geographic information;

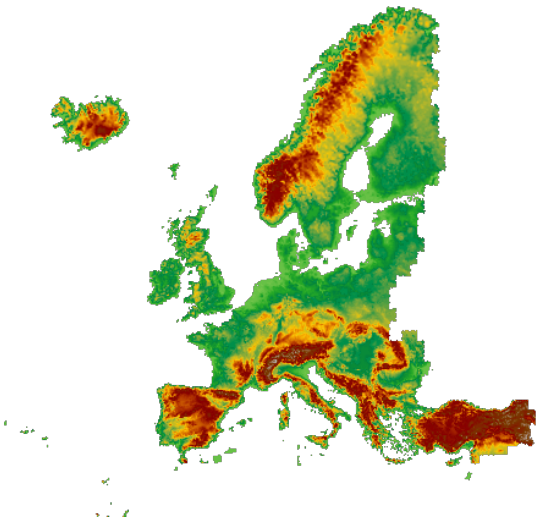

Figure 2.2: Land monitoring service
Source: [57]

- **Sentinel-2**: Marine monitoring changes;

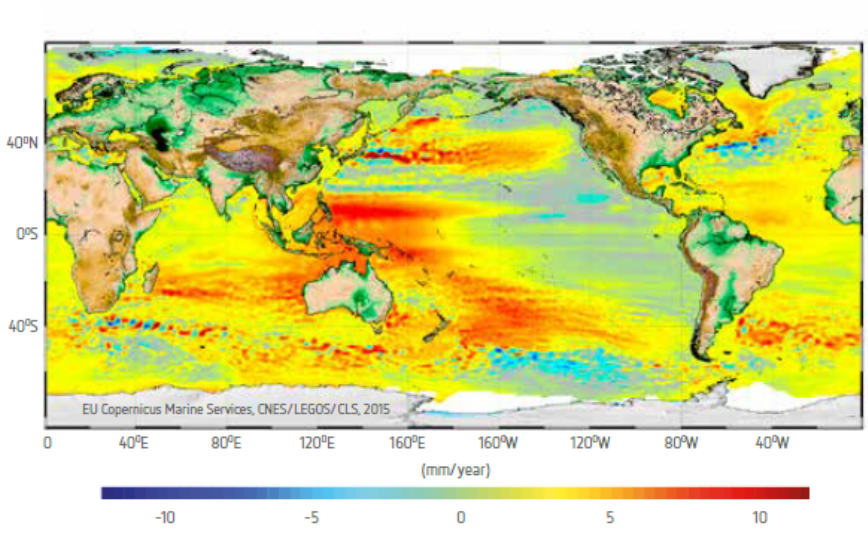

Figure 2.3: Marine monitoring service
Source:[58]

- **Sentinel-3**: Atmosphere monitoring changes;

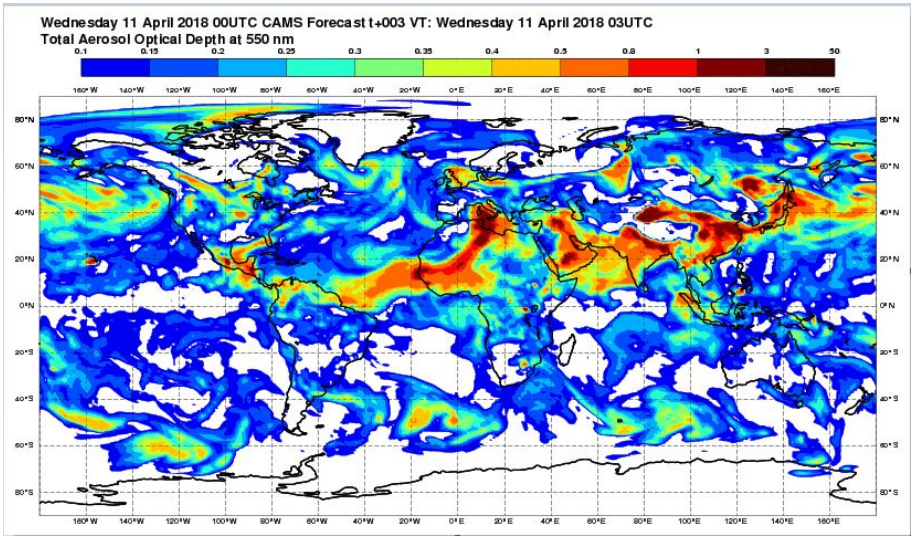

Figure 2.4: Land monitoring service
Source: [59]

- **Sentinel-4**: Climate monitoring changes;

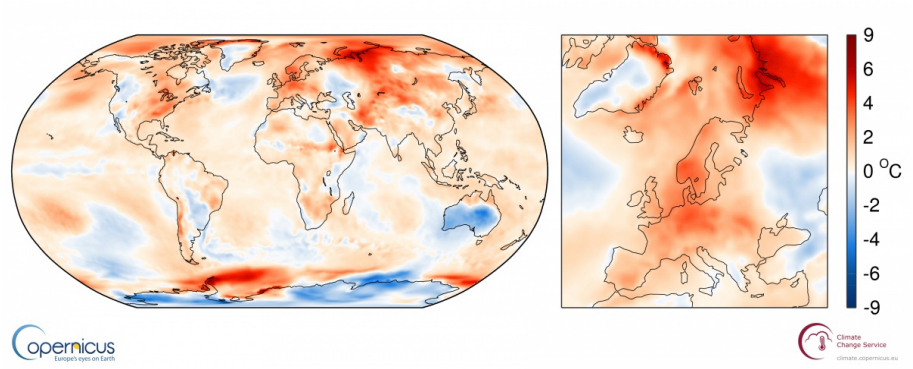

Figure 2.5: Climate monitoring service
Source: [60]

- **Sentinel-5**: Emergency management service;

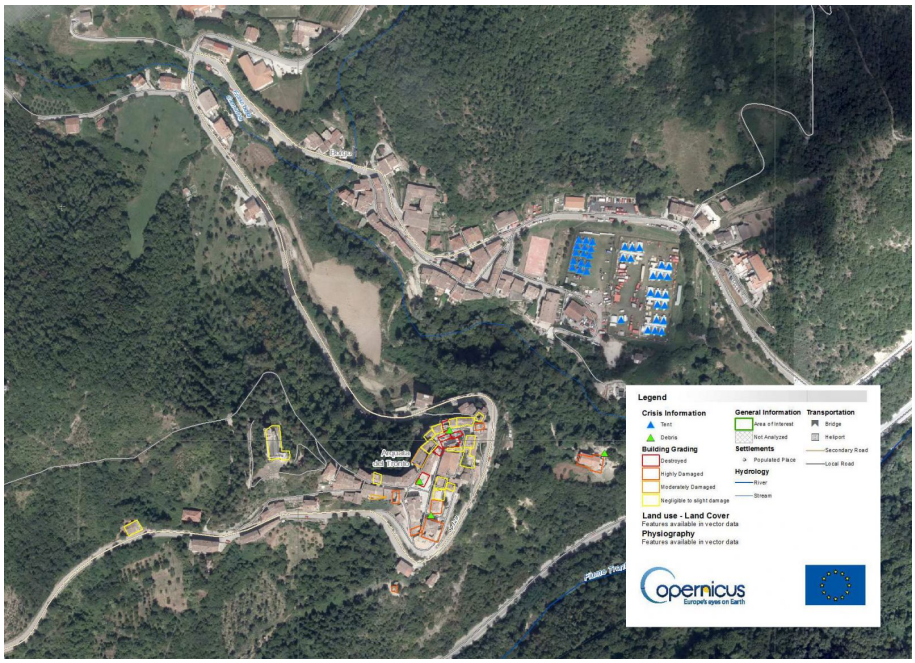

Figure 2.6: Emergency
Source: [61]

- **Sentinel-6**: security service;

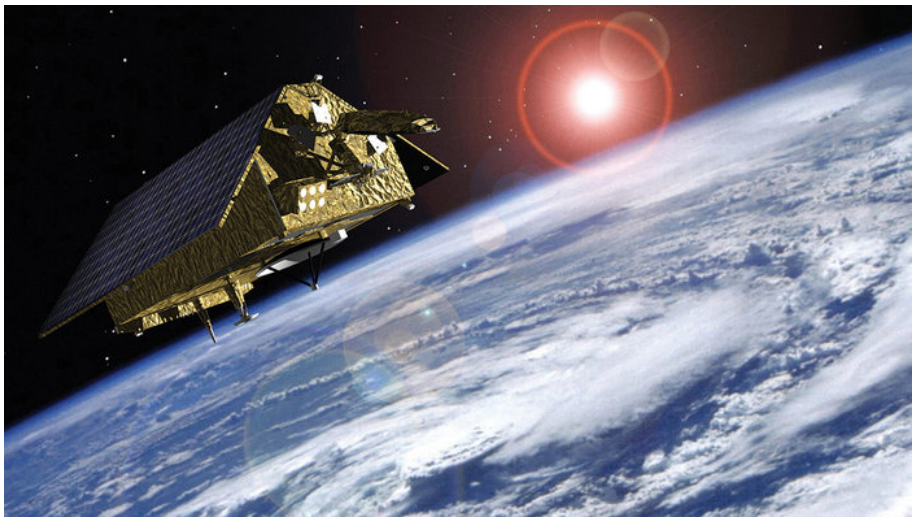

Figure 2.7: Sentinel-6
Source: [62]

- **EarthCARE**: Earth Cloud Aerosol and Radiation Explorer satellite mission;

Figure 2.8: Sentinel-6
Source: [63]

2.2 Sun-Synchronous Orbit

Sun-synchronous orbit allow the satellite pass in the same area of the Earth at the same solar time and ranges from 200 to 1680 km altitude wise and passes near the poles[50]. This type of orbit in relation to the sun is fixed. Whereas that Earth does a complete turn around the sun (360^o) per year, the spacecraft move 1^o per day to compensate. Sun-synchronous orbit is useful for mapping, weather satellites and communication satellites.

For the spacecraft to have an sun-synchronous orbit it needs to maintain a height and the respective orbital inclination. If one of this parameters changes the spacecraft no longer have a sun-synchronous orbit.

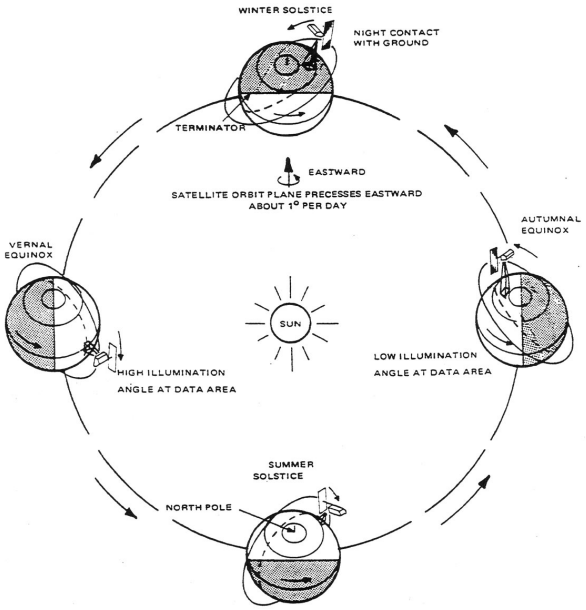

Figure 2.9: Sun-synchronous orbit.
Source: [64]

2.2.1 Coordinate Frames

To represent the different types of objects, for example Moon, Earth and satellite, we have a diversity of coordinates frames.

- **Earth-centered Inertial (ECI)**- Their origin is at the center of Earth.

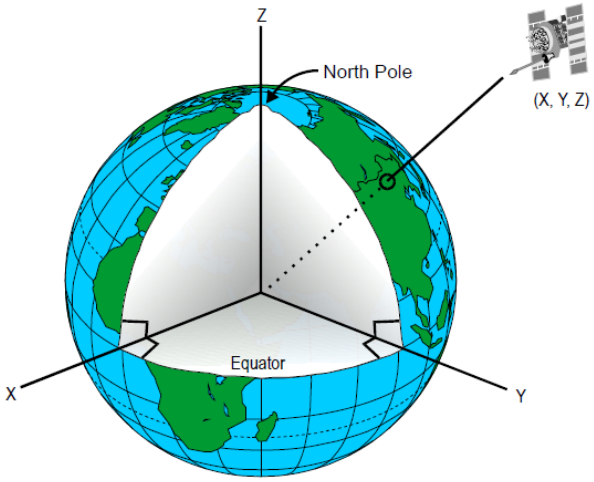

Figure 2.10: Example of Earth-centered Inertial frame.
Source: [65]

- **Earth-centered Earth-fixed (ECEF)**- Like ECI, their origin is at the center of Earth, but now the x-axis and y-axis rotate with same angular velocity as Earth. In other words, the coordinates at a given fixed point does not change with the rotation of the Earth.

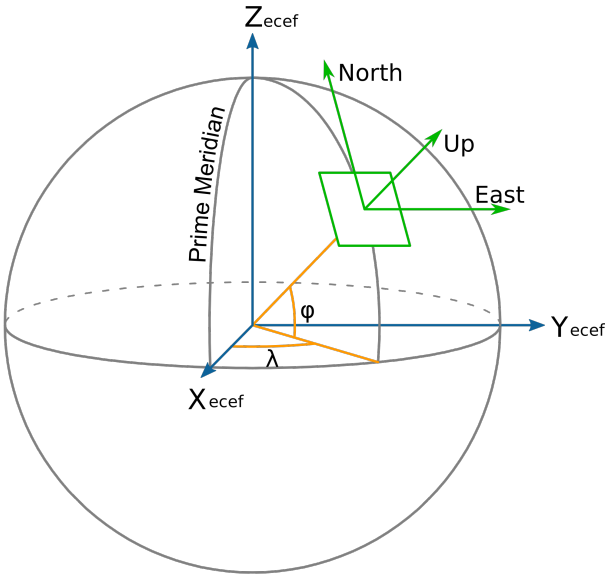

Figure 2.11: Example of Earth-centered Earth-fixed frame.
Source: [66]

- **Orbit Satellite frame**- Their origin is at the center of satellite, where the x-axis represents the direction of the velocity of the satellite, z-axis point to the center of the Earth and the y-axis completes the set of coordinates axis.

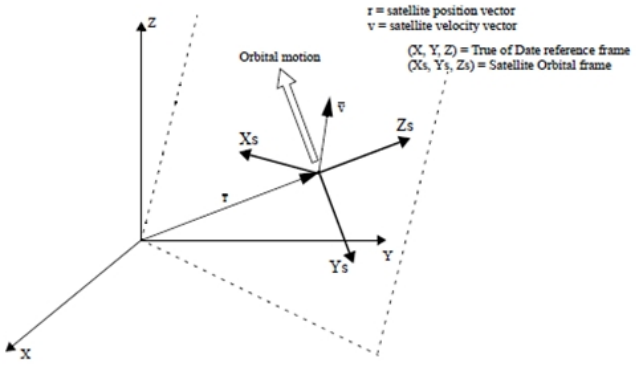

Figure 2.12: Example of Orbit frame.
Source: [67]

- **Satellite Body frame**- Their origin is at the center of satellite and it is useful to represent the satellite in space.

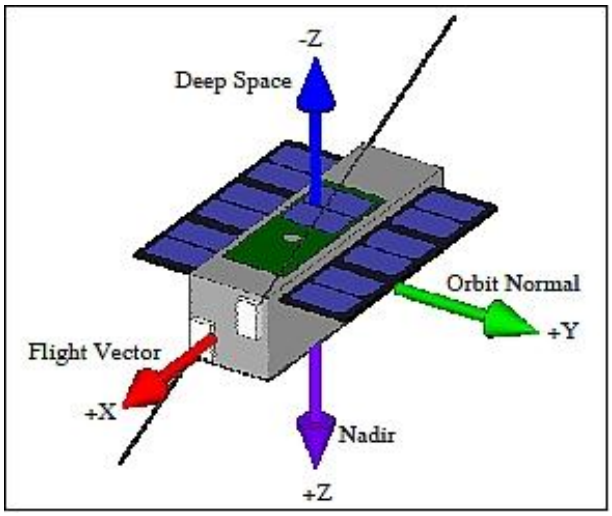

Figure 2.13: Example of Orbit frame.
Source:[68]

2.2.2 Coordinate Transformations

A coordinate transformation is a mapping that relates the representation in one coordinate system to another. For example, transforming a Cartesian coordinate system into another coordinate system is done by rotating on each of the coordinate axes. In that case, the three rotational matrices are:

$$P_x(\alpha) = \begin{bmatrix} 1 & 0 & 0 \\ 0 & \cos\alpha & \sin\alpha \\ 0 & -\sin\alpha & \cos\alpha \end{bmatrix} \tag{2.1}$$

$$P_y(\alpha) = \begin{bmatrix} \cos\alpha & 0 & -\sin\alpha \\ 0 & 1 & 0 \\ \sin\alpha & 0 & \cos\alpha \end{bmatrix} \tag{2.2}$$

$$P_z(\alpha) = \begin{bmatrix} \cos\alpha & \sin\alpha & 0 \\ -\sin\alpha & \cos\alpha & 0 \\ 0 & 0 & 1 \end{bmatrix} \tag{2.3}$$

where α corresponds to the counter-clockwise angle on each axis.

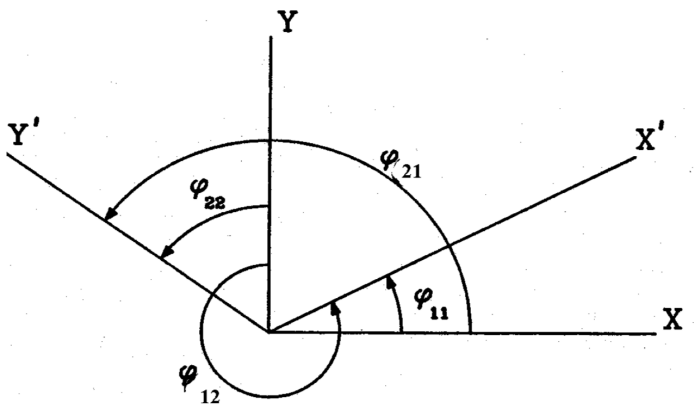

Figure 2.14: Coordinate frames related.
Source: [31]

2.2.3 Injection Trajectory and angular velocity

To be in orbit, the spacecraft needs to have an injection trajectory and an angular velocity.

To determine the relative position of Earth, Moon and Sun we need to know a calendar date, the injection of the spacecraft and the angular velocity.

With the specified calendar date we can know the altitude and inclination of spacecraft. It is necessary to have an angular velocity to maintain the height and control spacecraft orbit's.

The injection trajectory is the trajectory that spacecraft will make until it arrive to the planet or near-Earth object (NEOs). For example, if we want the spacecraft to arrive to Mars the injection trajectory will trace the route that the spacecraft will make.

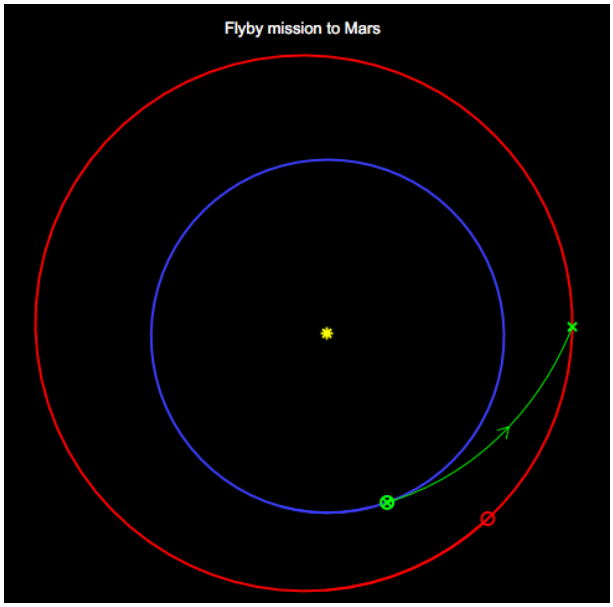

Figure 2.15: Example of injection trajectory.
Source: [69]

2.2.4 CESS

The Coarse Earth Sun Sensor (CESS) provides an omnidirectional coarse estimation of Earth and Sun position in the satellite reference frame [44].

CESS have two sensors, thermistors, which heat in different ways when they are exposed to solar or infrared emissions emitted by Sun and reflected by Earth, Earth Albedo. The output of CESS is given in *Ohms*.

The Earth Albedo is the reflecting power of a surface and it has a scale from zero to one. The lower *albedo* is, the more sun radiation is absorbed. As well as, the bigger *albedo* is, the less sun radiation is absorbed. The *albedo* allows scientists to study climate change and the changes in the Earth's surface [70].

Furthermore, from the study of *albedo*, we can know some properties of planets or asteroids. For example, one can find out the type of surface and this way, if there is ice outside the Earth.

Figure 2.16: Example of a CESS.
Source: http://www.spacetech-i.com/products/satellite-equipment/cess-a-cess

To determine the relative position of Earth and Sun vector, the CESS uses six orthogonal axis, while measures the temperatures and estimate the irradiated infrared emissions and solar flux.

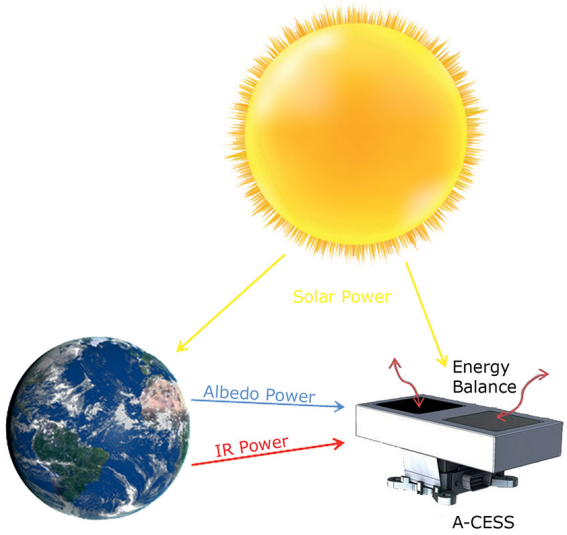

Figure 2.17: How the CESS works.
Source: http://www.spacetech-i.com/products/satellite-equipment/cess-a-cess

2.2.5 Star Tracker

The *Star Tracker* or simply STR is an optical attitude measurement devices [48] as CESS, however, the STR has more accuracy. Since ancient times, the humans used reference stars to help navigate. Nowadays, this is very useful to spacecraft navigation. Furthermore, there is a list of almost 57 stars that are ease of identification [71].

Figure 2.18: Example of star tracker.
Source: [72]

From an image captured from the stars, the STR can estimate the position in the reference frame of the spacecraft because of differences between the captured imaged with the stars and their absolute position from a star catalog [73].

To compute the altitude, inclination or angular velocity we need to observe the changes of star's positions relative to the satellite over time.

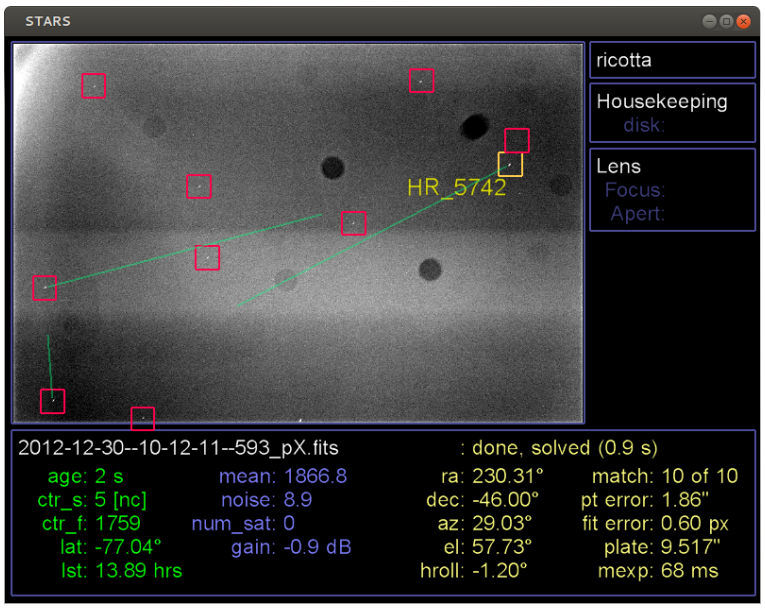

Figure 2.19: example of an image captured by STR.
Source: [73]

2.2.6 Earth Magnetic Field

Spacecraft in Earth orbit use magnetometers as attitude control sensors. The magnetometer is an sensor that measures the flux of the magnetic field.

To calculate the magnetic field in Cartesian coordinates, we need to know the spacecraft's coordinates in space (x, y, z). Also, we need to calculate the distance from spacecraft to the center of the Earth.

$$r = \left(x^2 + y^2 + z^2\right)^{\frac{1}{2}} \tag{2.4}$$

Also, we need to know radius of Earth (R) and the constant M, that it is equal to 31000 nT R^3.

$$B_x = \frac{3xzM}{r^5}; B_y = \frac{3yzM}{r^5}; B_z = \frac{\left(3z^2 - r^2\right)M}{r^5} \tag{2.5}$$

2.2.7 Nutation and Precession

Nutation and *Precession* are the motion of the Earth's axis and they are periodic [1].
The *Nutation* is the angle that the axis Earth's axis makes with the reference frame [1]. This motion is due to the gravitational attraction of Sun and Moon.

The *Precession* is a change in the orientation of the rotational axis of the Earth. In other words, *Precession* is the changes Earths rotational axis. Like *Nutation* the cause of the *Precession* is gravitational attraction of the Sun and Moon.

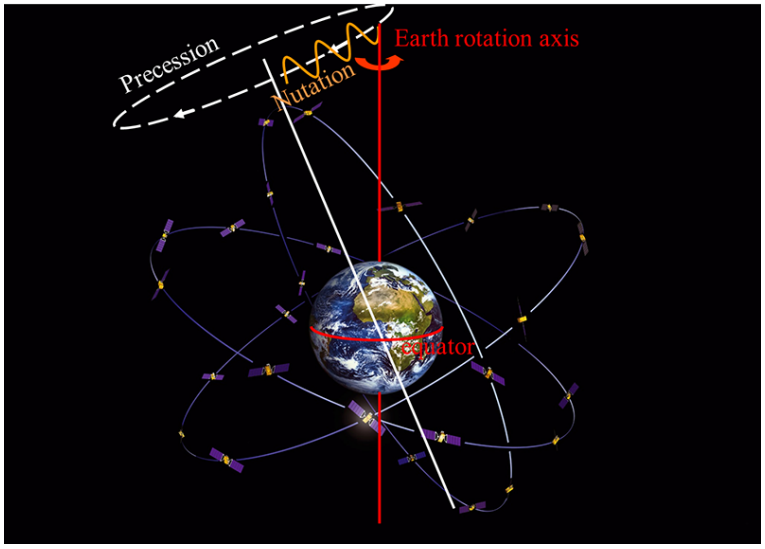

Figure 2.20: The difference between *Nutation* and *Precession*.
Source: [74]

2.2.8 Azimuth and Elevation

Over time the spacecraft in orbit needs to communicate with the *ground stations* to send or receive data. As *ground stations* are fixed to the ground it is essential to know the visibility windows between spacecraft and *ground stations*. The main telecommunications device of the *ground stations* is the parabolic antenna.

To calculate the visibility windowns between spacecraft and *ground stations* we need to know: *azimuth*, *elevation* and *great-circle distance*.

- **The azimuth** is the horizontal angular distance between the North and a star, measured in degrees [75].

$$\cos\alpha = \frac{-\sin h \cos\beta}{\sin\gamma} \tag{2.6}$$

In this case, we assume that the Earth is a sphere, α is the azimuth angle, the β is actual spacecraft declination, the γ is the zenith angle (is one point over the ground stations) and lastly, h is the hour angle.

- **The elevation** or altitude is the vertical angular distance between a star and the ground.

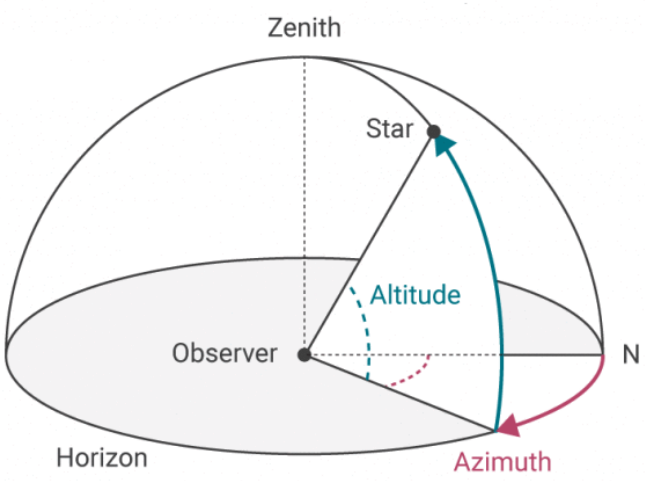

Figure 2.21: Elevation and azimuth.
Source: [76]

- **Great-circle distance** is the minimum distance between two points on the surface of the Earth. With great-circle distance we can calculate the visibility windowns between spacecraft and ground stations.

$$a = \sin^2\left(\frac{\Delta\phi}{2}\right) + \cos\phi_1 \times \cos\phi_2 * \sin^2\left(\frac{\Delta\lambda}{2}\right) \tag{2.7}$$

The ϕ is the latitude, λ is the longitude from one point, and $\Delta\phi$ and $\Delta\lambda$ are the difference, respectively, of the latitude and longitude between two points.

$$c = 2 \times \tan 2\left(\sqrt{a}, \sqrt{(1-a)}\right) \tag{2.8}$$

$$d = R \times c \tag{2.9}$$

2.3 Clean Space

As previously described, satellites are essential to our daily life and over the years the number of satellites is accumulating on Earth's orbit. Presently there are more than 6000 satellites in orbit. Between then, only less than an hundred are fully operational, that number corresponds 6% of all the satellites around the Earth. With time the satellites that are obsolete could explode and their fragments or mission-related objects are a problem for the next space missions. Therefore collisions between functional and obsolete satellites are a reality and this can cause even more space debris, can lead some missions to failure and that is very expensive. The space debris is a major risk for space missions [40] .

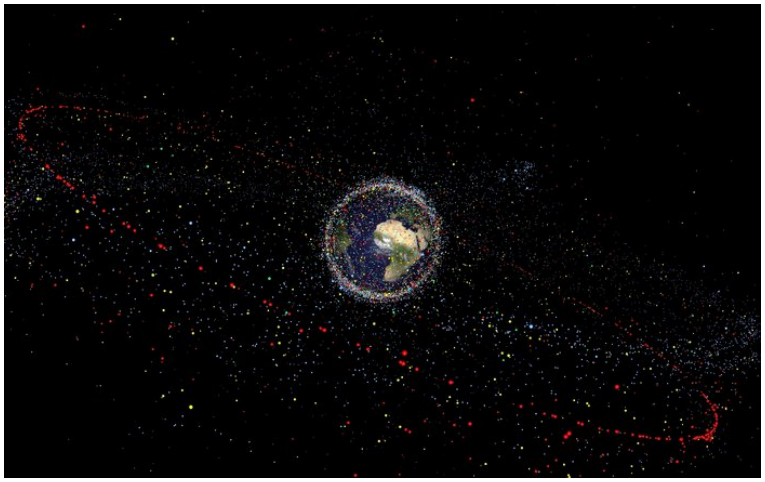

Figure 2.22: Satellites into Earth's orbit.
Source: [77]

ESA recently has an initiative to *clean space* so that space exploration could continue and there is no space debris. Thus, the three solutions proposed by Esa [78] are:

- **EcoDesign**: promote green technologies and and study environmental impacts;
- **CleanSat**:reduce production of space debris;
- **eDeorbit**: remove space debris from orbit;

e.Deorbit will be launched by 2023 and its main mission will be de-orbit debris with an altitude of less than 600 km, re-orbit debris with a altitude of more than 2000km and finally, allow the controlled re-entry of debris into the Earth's atmosphere that within 25 years debris does not decay.

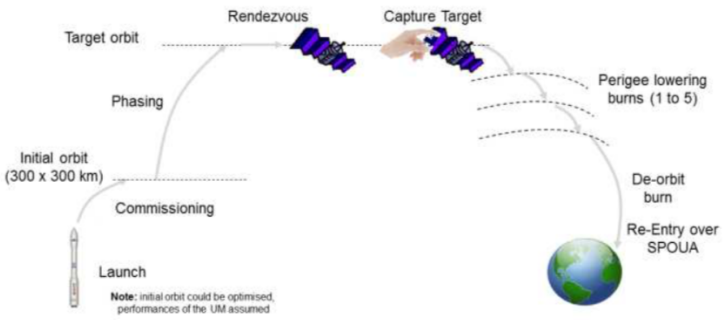

Figure 2.23: e.Deorbit mission.
Source: [79]

The target must not have a mass exceeding eight tonnes, it has to be obsolete and with sun-synchronous orbit. As the mission of *e.Deorbit* is to remove several targets, it must be able to evaluate several types of targets at a distance. For that it will need:

- navigational systems;
- cameras;
- propulsion system;
    1. chemical;
    2. electrical;
- capture technique (could be):
    1. robotic arm;
    2. tentacles;
    3. net;
    4. ion-beam shepherd;

In this Dissertation we will study the *e.Deorbit* solution, in particular the guidance navigation and control of *e.Deorbit* from phase that knows what the target is until its capture.
The target orbit is determined by RADAR sensors that are on the ground and when the *e.Deorbit* is relatively close to the target, the distance between the two is obtained through the relative navigation stars, [29].
When the spacecraft's LIDAR detects the target, the distance between them is approximately 1 km and the LIDAR measures the line of vision and the range [29].

2.4 5G- Satellites

The 5th generation wireless systems, also called 5G, is the next communications system. The 5G will have an higher bandwidth capacity, more secure communications and allows a greater number of users to have a data rate of 10Gb/s. Also, the 5G intends to have a latency lower than 4G and save the battery consumption.

The *5G-Satellites* will play a very important role in the implementation of 5G. For example, security, transport service, coverage and public safety. With 5G-satellites it is possible to provide communications in the most isolated areas but also guarantee communications in areas requiring additional capacity [39].

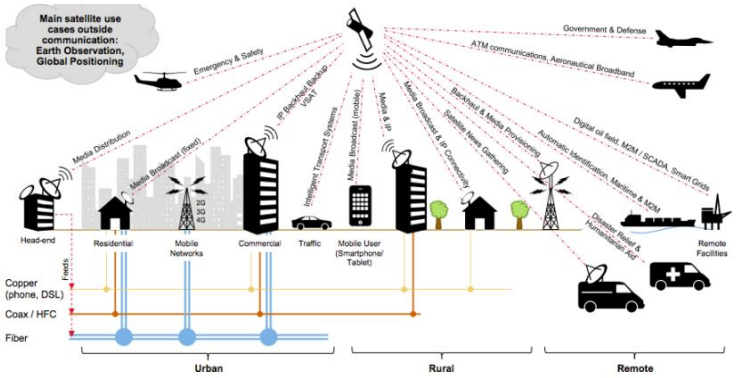

Figure 2.24: 5G-satellite
Source: [80]

The networks will have an higher speed due to use of millimeter wave band transmission. Notice that, data is transmited over radio waves and one of properties of electromagnetic waves is that the higher the frequency is, the smaller its wavelength is. Also, the higher the frequency the more data it can transmit. Therefore, the millimeter wave uses a band between the 30 GHz and 300 GHz so the wavelength is in the range of milimeters [24].

As previously stressed, satellites will play a very important role in the implementation of 5G technology, and in particular for:

- Coverage and integration;
- resilience;
- content multicast and caching;
- internet of things over satellite network;
- higher user mobility;

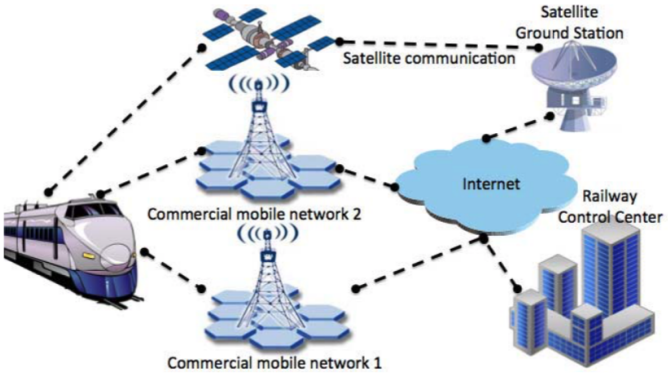

Figure 2.25: Network ecosystem
Source:[30]

With satellites it is possible to provide greater network coverage. If some terrestrial cells are at their maximum capacity through a network configuration software satellites can provide network to the cells [30].

Chapter 3

Orbit Dynamics

This chapter provides a brief survey of orbit dynamics. We start with the Kepler's laws, that provides a description of the motions of the planets in the solar system, but they do not explain why the planets move in that way. Next, we present the Newton's Universal Law of Gravitation that combined with the Newton's Laws of Motion can be used to explain the original Kepler's law.

3.1 The Kepler's Laws

Johannes Kepler began as Tycho Brahe's helper and student. During most of his life, *Tycho Brahe* recorded the positions of the planets over time. This recorded data turned out to be instrumental for the findings of Kepler. Indeed, when Kepler was analyzing the data, he found interesting relations, that are current summarized as the three laws of Kepler:

- **First Law:** The orbit of the planets around the sun is elliptical.

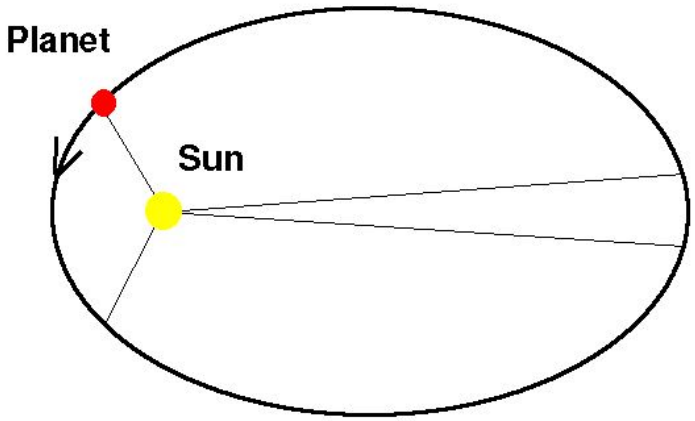

Figure 3.1: First Kepler Law
Source: [81]

See Fig. 3.1, where in this case the sun is the primary. The body that is centered with the reference point used is called as primary, while the other body is designated as secondary. The Kepler elements that characterize the trajectories (see Fig. 3.2) are used in non-inertial trajectories and centered on one of the bodies.

Keplerian elements:

- e - eccentricity of orbit;
  If **e** is equal to zero the orbit is a circle, or if **e** is between zero and one the orbit is an ellipse and for the last case, if **e** is bigger than one the orbit is a parable.
- α - semi-major axis of the planet's orbit;
- P - perihelion;
- i - angle between plane of the Sun's equator and planet's orbit;
- ω - longitude of perihelion;
- Ω - longitude of ascending node;

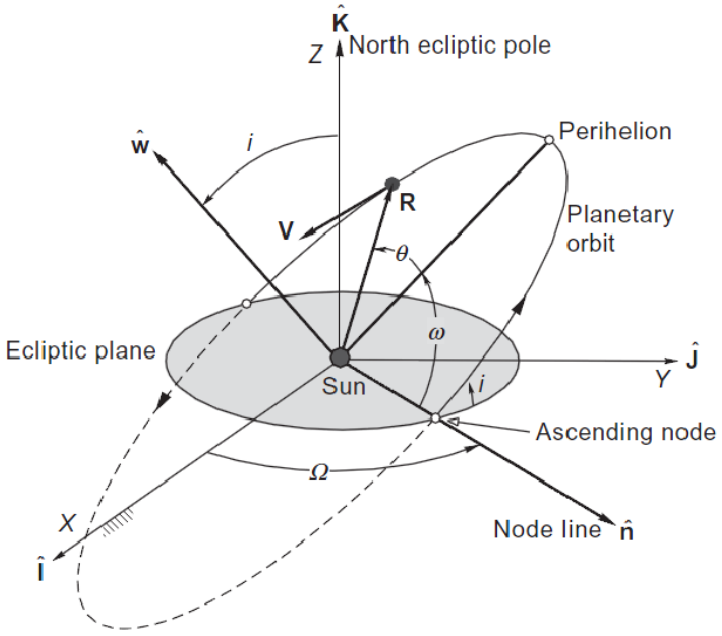

Figure 3.2: Kepler elements
Source: [11]

From the Kepler elements one can compute the distance from the planet to the sun. To this effect, we need to perform the following calculations.

First, we need to calculate the eccentric anomaly. Considering that the equation of an ellipse is given by,

$$\frac{x^2}{a^2} + \frac{y^2}{b^2} = 1 \tag{3.1}$$

It follows that,

$$\cos(E) = \frac{x}{a} \tag{3.2}$$

and

$$\sin(E) = \frac{y}{b}, \tag{3.3}$$

where E is the eccentric anomaly, a is the semi-major axis and b is the semi-minor axis.

From this, the mean anomaly (denoted by M) and the angle of planet from perihelion (denoted by ν) are obtained as:

$$M = E - \mathbf{e}\sin(E) \tag{3.4}$$

$$\nu = 2\tan^{-1}\left(\sqrt{\frac{1+\mathbf{e}}{1-\mathbf{e}}}\tan\left(\frac{E}{2}\right)\right) \tag{3.5}$$

Lastly, the calculation of the distance between the planet and the Sun, denoted by r, is given by

$$r = \frac{a\left(1-\mathbf{e}^2\right)}{1+\mathbf{e}\cos\nu}, \tag{3.6}$$

- **Second Law:** A line segment joining a planet and the Sun sweeps out equal areas during equal intervals of time, see Fig. 3.3. This means that the orbit velocity of the planet is not constant, but the *area speed* is constant.

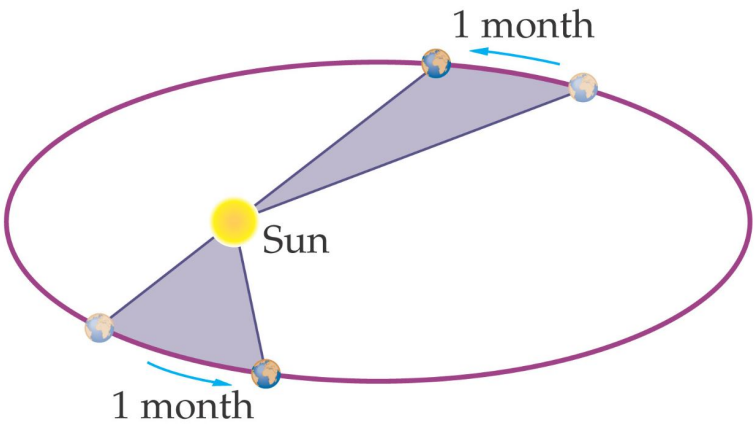

Figure 3.3: Second Kepler Law
Source: [82]

- **Third Law:** The square of the orbital period T of a planet is proportional to the the cube of the semi-major axis of the orbit of the planet, that is,

$$T^2 \propto a^3 \tag{3.7}$$

Satellite's Position

To find the position of a satellite with the Kepler's Laws using the Heliocentric Ecliptic coordinates (x, y, z) one get,

$$x = r(\cos(\Omega)\cos(\omega+\nu) - \sin(\Omega)\sin(\omega+\nu)\cos(i)) \tag{3.8}$$

$$y = r(\sin(\Omega)\cos(\omega+\nu) + \cos(\Omega)\sin(\omega+\nu)\cos(i)) \tag{3.9}$$

$$z = r\sin(\Omega)\sin(\omega+\nu)\cos(i) \tag{3.10}$$

To obtain in the Heliocentric Equatorial coordinates(X,Y,Z), we need to perform the following transformation

$$\begin{bmatrix} X \\ Y \\ Z \end{bmatrix} = \begin{bmatrix} 1 & 0 & 0 \\ 0 & \cos(i) & -\sin(i) \\ 0 & \sin(i) & \cos(i) \end{bmatrix} \begin{bmatrix} x \\ y \\ z \end{bmatrix} \tag{3.11}$$

Although Kepler's laws were an advance for the study of the satellite's orbit, these laws are based on data that Tycho Brahe registered to that of time [83] and as such do not explain why the

orbits of the planets move in this way.

3.2 The Newton's Laws

Years later, in 1687, Isaac Newton presented his Universal Law of Gravitation through Kepler's Third Law.

3.2.1 Newton's Universal Law of Gravitation

The Newton's universal equation of gravity says basically that the force F of attraction between two bodies of mass M and m is proportional to the product of the two masses, and inverse proportional to the square of the distance r between them. For the example case of Earth with mass M and Moon with mass m, one has

$$F = G\frac{mM}{r^2}, \tag{3.12}$$

where, G is the gravitational constant the value 6.670×10^{-11}. and r is the distance between Moon and the Earth.

Third Law of Kepler from Newton's Universal Law of Gravitation

Kepler's third Law can be derived from applying the Laws of Motion and Newton's universal equation of gravity. We can see more in detail at [2].

For simplify the calculation it consider that the rigid body has a circular orbit around the Earth. Applying the Laws of Motion on the rigid body in circular motion this force is denoted by centripetal force:

$$F_c = m\frac{v^2}{R}, \tag{3.13}$$

where, the mass of the rigid body is denoted by m, the orbital velocity is denoted by v and distance R in the circular motion is the semi-major axis a.

As the motion of the rigid body is circular, the velocity can be described by the space traveled to divided by the time that the rigid body takes to take a turn. Following, the space traveled can be defined by 2π R, where R is the distance from rigid body to the Earth.

$$v = \frac{2\pi R}{T} \tag{3.14}$$

If we equate the gravitational force with the centripetal force one get,

$$G\frac{Mm}{R^2} = \frac{mv^2}{R} \tag{3.15}$$

If we resolve the last equation in function of period, T, is given by,

$$T^2 = \frac{4\pi^2}{G(M+m)}R^3, \tag{3.16}$$

where, T is the period of the rigid body (in Earth years).

3.3 Simulation Results

In this Section we illustrate through computer simulations the evolution of the satellite's position relative to the Earth.

Through the tool developed by NASA called by *General Mission Analysis Tool*, GMAT, it was simulated the satellite sun-synchronous orbit around the Earth over a period of one day.
The results obtained for the satellite's position (see figures 3.4 and 3.5) has as reference point the center of the Earth.

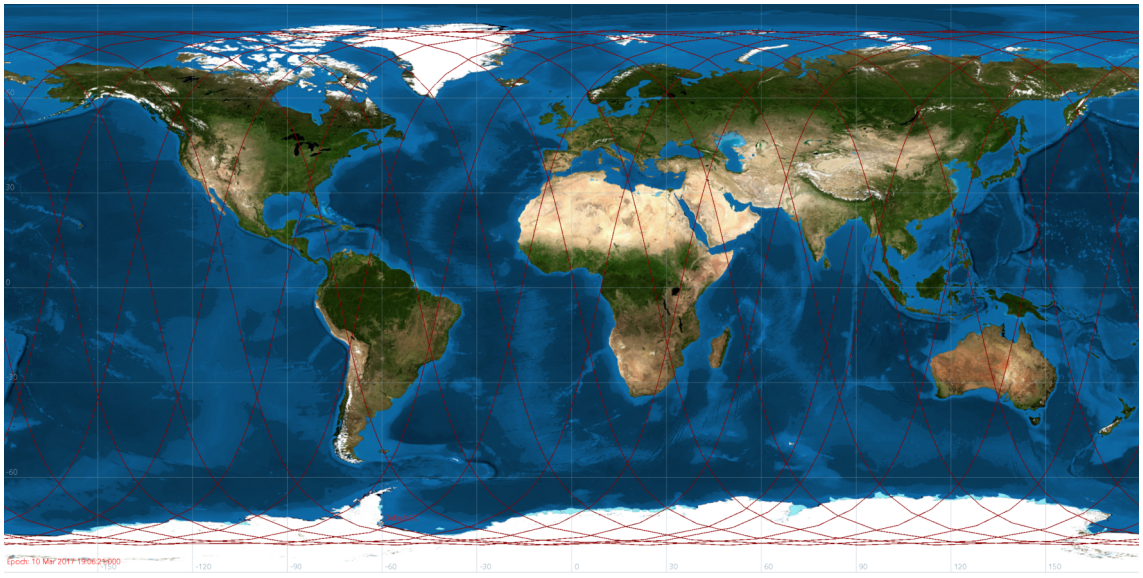

Figure 3.4: Satellite with a sun-synchronous orbit.

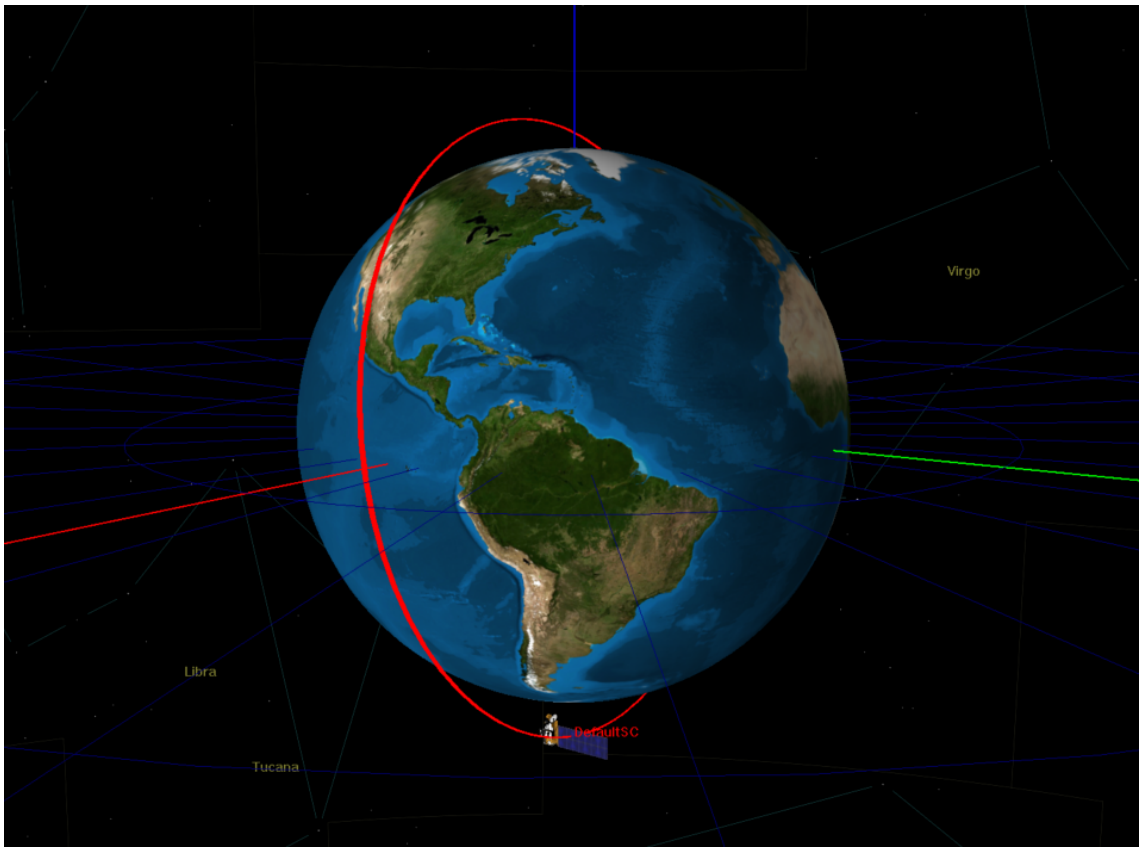

Figure 3.5: Sun-synchrnous satellite around the Earth.

The following figures show the positions of the satellite relative to the center of the Earth. In the figure 3.7, the result obtained was through the OpenModelica tool.

The distance of the satellite from the center of the Earth (denoted by r) throught Newton's laws is given by,

$$r = \frac{\frac{L^2}{GMm^2}}{1 + e\cos\theta} \tag{3.17}$$

where, L is the angular momentum of the satellite, mass of the Earth is denoted by M and the mass of satellite is denoted by m. It possible see the deduction of the equation (3.17) in [4]. Also, note that the angular momentum of a satellite is calculate by the equation (4.14).

The results obtained for the position of the satellite in relation to the Earth.

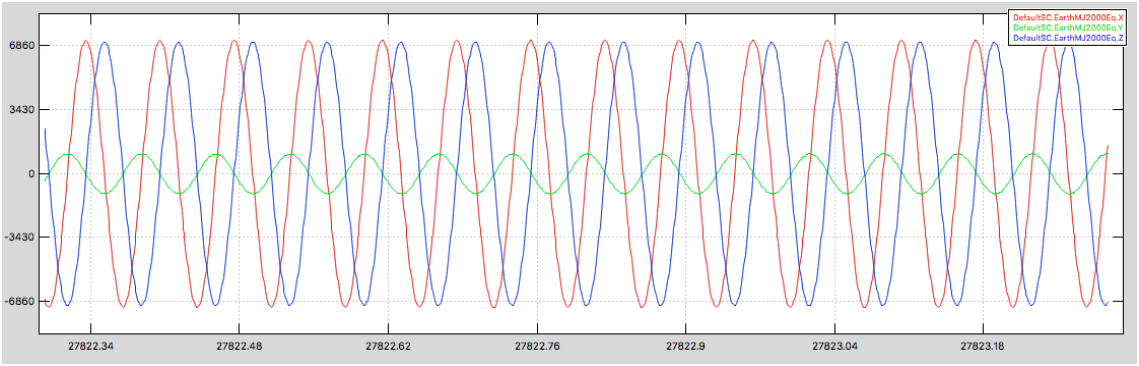

Figure 3.6: Satellite position.

The following are the results of the distance of the satellite from the center of the Earth through Newton's laws.

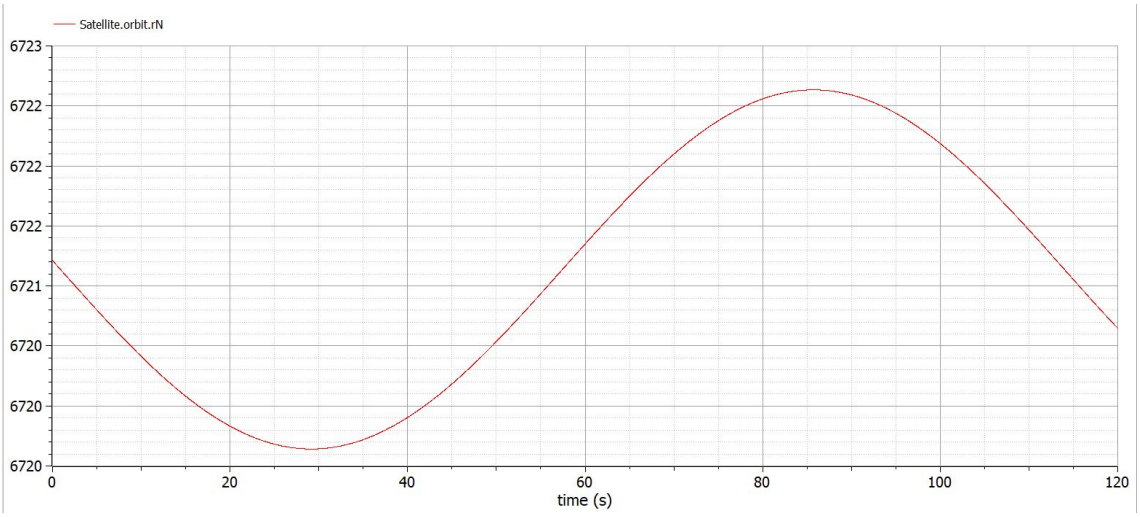

Figure 3.7: Satellite distance relative to the center of the Earth with the Newton Laws.

See figure 3.7, the distance changes along the time because Newton's Laws takes into account the forces applied to the satellite. Contrary, the Kepler's Laws are based on collected data and the distance is constant along the time.

Chapter 4

Spacecraft Kinematics and Dynamics

This chapter is dedicated to the kinematics and dynamics of a spacecraft.
In Section 4.1 we present the attitude kinematics of a spacecraft. The attitude kinematics is represented first by *Euler angles* and after by *quaternion*. Section 4.2 is dedicated to the spacecraft's dynamic. To calculate attitude dynamic of spacecraft it is used angular momentum, rigid body dymamics and motion and Euler's equation of motion. In Section 4.3 we present the actuators that create the internal torques of the spacecraft, and finally in Section 4.4 we present the actuators that create the external torque of the spacecraft.

4.1 Attitude kinematics of a spacecraft

This Section introduces the two main representation of the attitude of a spacecraft: Euler Angle Kinematics and Quaternion Kinematics.

4.1.1 Euler Angle Kinematics

Euler angle is used to represent a rotation of the spacecraft. Representing the attitude kinematics by the Euler angle is easier to develop and to visualise but it uses a lot of computational power. And it is not successful method to describe attitude dynamics of a spacecraft. We can see the deduction of the Euler angle kinematics in [12].

$$\begin{bmatrix} \dot{\theta}_1 \\ \dot{\theta}_2 \\ \dot{\theta}_3 \end{bmatrix} = \frac{1}{\cos\theta_2} \begin{bmatrix} \cos\theta_2 & \sin\theta_1 \sin\theta_2 & \cos\theta_1 \sin\theta_2 \\ 0 & \cos\theta_1 \cos\theta_2 & -\sin\theta_1 \cos\theta_2 \\ 0 & \sin\theta_1 & \cos\theta_1 \end{bmatrix} \begin{bmatrix} \omega_1 \\ \omega_2 \\ \omega_3 \end{bmatrix} \tag{4.1}$$

where, the ω is the angular velocity, θ are the angular positions.

4.1.2 Quaternion Kinematics

Quaternion representation have four components vector. The quaternion (denoted by q) has two parts, the first part consists of three-vector part and a scalar part, that is,

$$q = \begin{bmatrix} q_{1:3} \\ q_4 \end{bmatrix} \tag{4.2}$$

where

$$q_{1:3} = \begin{bmatrix} q_1 \\ q_2 \\ q_3 \end{bmatrix} \tag{4.3}$$

The representation of the quaternions is based on the Euler rotational theorem. Representing the attitude kinematics by quaternions there are several advantages for example, to the successive rotations can be resolved by quaternions multiplicative [13] and [10]. To determine the attitude of spacecraft it is necessary to integrate the quaternions kinematic equation

$$\begin{bmatrix} \dot{q}_1 \\ \dot{q}_2 \\ \dot{q}_3 \\ \dot{q}_4 \end{bmatrix} = \frac{1}{2} \begin{bmatrix} 0 & \omega_3 & -\omega_2 & \omega_1 \\ -\omega_3 & 0 & \omega_1 & \omega_2 \\ \omega_2 & -\omega_1 & 0 & \omega_3 \\ -\omega_1 & -\omega_2 & -\omega_3 & 0 \end{bmatrix} \begin{bmatrix} q_1 \\ q_2 \\ q_3 \\ q_4 \end{bmatrix} \tag{4.4}$$

where, the angular velocity, denoted by ω, evolves according to the by dynamics equations.

The compact form to represent the quaternion kinematics of the satellite is

$$\dot{q} = \frac{1}{2}\Omega(\omega)q \tag{4.5}$$

so that,

$$\Omega(\omega) = \begin{bmatrix} -[\omega\times] & \omega \\ -\omega^T & 0 \end{bmatrix} \tag{4.6}$$

4.2 Attitude Dynamics

Angular Momentum

In order to obtain the angular acceleration we need to compute the angular momentum.

To calculate the angular momentum (denoted by H) of the spacecraft, first it is necessary to compute the momentum of inertia matrix (denoted by I). The momentum of inertia matrix is the inertia (difficulty of motion) of the body has to rotation around the axis.

The moment of inertia matrix is given by

$$I = \begin{bmatrix} I_{xx} & -I_{xy} & -I_{xz} \\ -I_{yx} & I_{yy} & -I_{yz} \\ -I_{zx} & -I_{zy} & I_{zz} \end{bmatrix} \tag{4.7}$$

where the components of moment of inertia matrix are given by,

$$I_{xy} = I_{yx} = \int\int\int xydm \tag{4.8}$$

$$I_{xz} = I_{zx} = \int\int\int xzdm \tag{4.9}$$

$$I_{yz} = I_{zy} = \int\int\int yzdm \tag{4.10}$$

$$I_{xx} = \int\int\int (y^2 + z^2)dm \tag{4.11}$$

$$I_{xz} = \int\int\int (x^2 + z^2)dm \tag{4.12}$$

$$I_{xz} = \int\int\int (y^2 + x^2)dm \tag{4.13}$$

From the moment of inertia, I, and the angular velocity of the satellite denoted by ω, we obtain the angular momentum as

$$\begin{bmatrix} H_x \\ H_y \\ H_z \end{bmatrix} = \begin{bmatrix} I_{xx} & -I_{xy} & -I_{xz} \\ -I_{yx} & I_{yy} & -I_{yz} \\ -I_{zx} & -I_{zy} & I_{zz} \end{bmatrix} \begin{bmatrix} \omega_x \\ \omega_y \\ \omega_z \end{bmatrix} \tag{4.14}$$

Euler's equation of motion

Using a body fixed reference to the satellite, we can now apply the Euler's equation of motion [9],

$$\begin{bmatrix} L \\ M \\ N \end{bmatrix} = \frac{d\vec{H}}{dt}|_B + \vec{\omega} \times \vec{H} \tag{4.15}$$

$$= \begin{bmatrix} I_{xx} & -I_{xy} & -I_{xz} \\ -I_{yx} & I_{yy} & -I_{yz} \\ -I_{zx} & -I_{zy} & I_{zz} \end{bmatrix} \times \begin{bmatrix} \dot{\omega}_x \\ \dot{\omega}_y \\ \dot{\omega}_z \end{bmatrix} + \begin{bmatrix} I_{xx} & -I_{xy} & -I_{xz} \\ -I_{yx} & I_{yy} & -I_{yz} \\ -I_{zx} & -I_{zy} & I_{zz} \end{bmatrix} * \begin{bmatrix} \omega_x \\ \omega_y \\ \omega_z \end{bmatrix} \tag{4.16}$$

$$= \begin{bmatrix} +I_{xx}\dot{\omega}_x - I_{xy}\dot{\omega}_y - I_{xz}\dot{\omega}_z \\ -I_{yx}\dot{\omega}_x + I_{yy}\dot{\omega}_y - I_{yz}\dot{\omega}_z \\ -I_{zx}\dot{\omega}_x - I_{zy}\dot{\omega}_y + I_{zz}\dot{\omega}_z \end{bmatrix} + \vec{\omega} \times \begin{bmatrix} +\omega_x I_{xx} - \omega_y I_{xy} - \omega_z I_{xz} \\ -\omega_x I_{yx} + \omega_y I_{yy} - \omega_z I_{yz} \\ -\omega_x I_{zx} - \omega_y I_{zy} + \omega_z I_{zz} \end{bmatrix} \tag{4.17}$$

$$= \begin{bmatrix} I_{xx}\dot{\omega}_x - I_{xy}\dot{\omega}_y - I_{xz}\dot{\omega}_z + \omega_y(\omega_z I_{zz} - \omega_x I_{xz} - \omega_y I_{yz}) - \omega_z(\omega_y I_{yy} - \omega_x I_{xy} - \omega_z I_{zz}) \\ I_{yy}\dot{\omega}_y - I_{xy}\dot{\omega}_x - I_{yz}\dot{\omega}_z - \omega_x(\omega_z I_{zz} - \omega_y I_{yz} - \omega_x I_{xz}) + \omega_z(\omega_x I_{xx} - \omega_y I_{xy} - \omega_z I_{xz}) \\ I_{zz}\dot{\omega}_z - I_{xz}\dot{\omega}_x + I_{yz}\dot{\omega}_y + \omega_x(\omega_y I_{yy} - \omega_x I_{xy} - \omega_z I_{yz}) - \omega_y(\omega_x I_{xx} - \omega_y I_{xy} - \omega_z I_{xz}) \end{bmatrix} \tag{4.18}$$

where, $\dot{\omega}$ is the angular acceleration of the satellite in the body frame.

To simplify the calculation, we consider that the moment of inertia of the spacecraft has two planes of symmetry [8], which implies

$$I_{yz} = I_{xy} = I_{xz} = 0 \tag{4.19}$$

The forme simplify of *Euler's equation* is given by,

$$\begin{bmatrix} L \\ M \\ N \end{bmatrix} = \begin{bmatrix} I_{xx}\dot{\omega}_x + \omega_y\omega_z(I_{zz} - I_{yy}) \\ I_{yy}\dot{\omega}_y + \omega_x\omega_z(I_{xx} - I_{zz}) \\ I_{zz}\dot{\omega}_z + \omega_x\omega_y(I_{yy} - I_{xx}) \end{bmatrix} \tag{4.20}$$

4.3 Internal Torques

Internal torques are created by the spacecraft actuators causing a change in angular momentum.

In this dissertation we consider for the actuators the reaction wheels and thrusters that create internal torques. Reaction wheels are commonly used for attitude control while the thrusters are used to orbit control.

4.3.1 Reaction Wheels

In order to determine the total angular momentum of the spacecraft with the reaction wheels we need to calculate the moment of inertia of the spacecraft with and without the wheels. The wheels are distinguish by l and considering that are n reaction wheels in the spacecraft.

Each reaction wheel rotates around the spin axis, thus the wheel is axially symmetric about its spin axis [12].

The equation for the calculation of the moment of inertia of wheel (denoted by J_l^w) is given by

$$J_l^w = J_l^{\perp}(I_3 - w_l w_l^T) + J_l^{\parallel} w_l w_l^T, \tag{4.21}$$

where w_l is the unit vector that defines the spin axis relative to the body frame, I_3 is the 3×3 identity matrix, $J_l^{\perp}$ and $J_l^{\parallel}$ are the moment of inertia perpendicular and parallel, respectively, to the spin axis.

To calculate the total moment of inertia with and without wheels we need to sum all the moment of inertia of the wheels and the moment of inertia of spacecraft without wheels, one get

$$J = \tilde{J} + \sum_{l=1}^{n} J_l^{\perp}(I_3 - \omega_l w_l^T) \tag{4.22}$$

and the angular momentum of the wheel, denoted by H^w, along the spin axes is given by,

$$H^w = \sum_{l=1}^{n} J_l^{\parallel}(w_l \omega + \omega_l^w) w_l \equiv \sum_{l=1}^{n} H_l^w w_l \tag{4.23}$$

Therefore, the total angular momentum, denoted by H, of the spacecraft is

$$H = \tilde{J}\omega + \sum_{l=1}^{n} J_l^w(\omega + \omega_l^w w_l) = J\omega + H^w \tag{4.24}$$

where, ω_l^w is the angular velocity of the wheel, ω is the angular velocity of the spacecraft, $\tilde{J}$ is the moment of inertia without wheels and J is the moment of inertia of the wheels just in the transverse spin axes and not along spin axes.

The first part of the equation, see equation (4.22), corresponds to moment of inertia of the spacecraft without the wheels and the second part is the moment of inertia of wheels.

The torque applied by reaction wheels to the spacecraft is given by,

$$\dot{H}^w = \sum_{l=1}^{n} \dot{H}_l^w w_l = \sum_{l=1}^{n} L_l^w w_l \equiv L^w \tag{4.25}$$

The rotation kinetic energy, denoted by E_c of a spacecraft with the reaction wheels is given by,

$$E_c = \frac{1}{2}(\omega)^T J\omega + \frac{1}{2}\sum_{l=1}^{n}(J_l^{\|})^{-1}(H_l^w)^2 \tag{4.26}$$

4.3.2 Thruster

The thrusters are used to attitude control and orbit control, thus the torques (denoted by L) and forces (denoted by F) are applied on the spacecraft.

$$F = -\dot{m}v_{rel}, \tag{4.27}$$

and

$$L = r \times F \tag{4.28}$$

where $\dot{m}$ is the fuel mass loss rate, v_{rel} is the velocity of the removed mass relative to the spacecraft, r is the vector distance of the thruster to the spacecraft center of mass.

See in equation (4.27), the reaction force is on the spacecraft, so with the third law of motion the sign is negative.

4.4 External Torques

External torques are created by different mechanisms external to the spacecraft. In this dissertation we only consider magnetic dipole that create external torques.

4.4.1 Magnetic Torque

In order to calculate the torque (denoted by L) one need to compute the magnetic dipole (denoted by m), which is given by

$$m = NIA, \tag{4.29}$$

where, the number of wire loops is denoted by N, I is the current in amperes[A] and A is the area of the wire loop.

Now it is possible to determine the torque generated by magnetic dipole in body frame,

$$L = m \times B \tag{4.30}$$

Note that the magnetic torques can only control two axis each time. In other hand, the magnetic torques do not create forces thus they do not change the orbit of the spacecraft.

Chapter 5

Filtering for Attitude Estimation and Calibration

This chapter is dedicated to the attitude estimation of a spacecraft using the filter estimation. Section 5.1 provides a review of estimation theory, the differences between static-based and filter-based estimation. Also, it reviews some filter estimations, for instance the Kalman filter for linear systems and the extended Kalman filter for nonlinear systems. We will focus on the filter estimation because the model of the system is a dynamic model. Section 5.2 presentes three different representations of spacecraft attitude: three-component representations, additive quaternion representation and multiplicative quaternion representations as well as the advantages and disadvantages for different possibilities for the representations. In Section 5.3 we will see the description of the implementation and the differences between the Extended Kalman Filter and the Murrell's version. Lastly, Section 5.4 presents the simulation results for the attitude estimation of a spacecraft.

5.1 Background

This Section provides a brief review of estimation theory in the context of this dissertation as well, the differences between the estimations methods for linear and nonlinear systems. All methods of the estimation requires the sensor measurements to estimate unknown variables.

5.1.1 Static-Based and Filter-Based Estimation

The filter-based estimation to determine the current state of a system needs the previous time state and the sensors measurements, for example, the magnetometers sensors. The measurements are usually has corrupted by noise, which will be assumed to be Gaussian random noise.

The filter estimation could be applied to filter noisy measurement observations and the estimation quantities [12].

The static estimation can be used for initial estimate on the filter estimation or to verify the results of the filter estimation.

The advantages of using the static-based estimation are the fact that usually require less computationally effort and the estimation is better approximated to the desired solution. The main disadvantage is the need to have for each time the full observability so that the solution can be computed without algebraic singularities [13].

The advantages of using filter-based estimation techniques are the fact that a solution can be determined when exist algebraic singularity situations. Because one can include another state estimation variables from the nearby past. In case of attitude determination of a spacecraft, biases are included into the state estimation. Also for the previous case, the estimate error covariances is added to the solution. The disadvantage is that to determine a solution it is necessary the previous state. Also, in the comparison with the static estimation the filter estimation is computationally slower [12].

The definition of the covariance matrix is each element of the matrix in the i^{th} row and j^{th} column is the covariance between the i^{th} and j^{th} variables. The diagonal elements of the matrix are the variance of this variable. The covariance between this two variables is a measure of the joint variability of two random variables.

5.1.2 State Estimation Techniques

This section will focus on the filter estimation because in this dissertation the goal is to determine the attitude estimation using the satellite dynamic model.

Linear Kalman Filter

For dynamical linear models it is frequent the use of Kalman Filter because is an optimal filter in the sense that it minimizes the mean square estimation error assuming Gaussian noise.

The Kalman filter applied to the linear dynamics state model

$$\dot{x}^{true} = Fx^{true} + Bu + Gw \tag{5.1}$$

with discrete measurements

$$y_k = Hx_k + v_k \tag{5.2}$$

where, F is the state matrix, B is the input matrix and the Gaussian white-noise is denoted by w, is shown in Table 5.1, that provides a synopsis of the implementation of the Kalman filter.

Table 5.1: Continuous-discrete linear Kalman filter.

Model	$\dot{x}^{true} = Fx^{true} + Bu + Gw$, where $w \sim N(0,Q)$ $y_k = Hx_k^{true} + v_k$, where $v_k \sim N(0,R_k)$
Initialize	$\hat{x}(t_0) = \hat{x}_0$ $P(t_0) = P_0$
Propagation	$\dot{\hat{x}} = F\hat{x} + Bu$ $\dot{P} = FP + PF^T + GQG^T$
Gain	$K_k = P_k^- H_k^T [H_k P_k^- H_k^T + R_k]^{-1}]$
Update	$\hat{x}^+ = \hat{x}^- + K_k[y_k - H_k\hat{x}^-]$ $P_k^+ = [I - K_k H_k]P_k^-$

In Table 5.1, the equations of the model have the Gaussian distribution for zero mean and spectral density Q is denoted by $w \sim N(0,Q)$ and $v_k \sim N(0,R_k)$ is the Gaussian distribution for zero mean and the covariance (designate by R). The initalization of the filter needs an initial state, $\hat{x}(t_0)$, and the inital error covariance, $P(t_0)$.

5.2 Attitude Representation for Kalman filtering

As we will see in this Section, one of the best options for the representation of spacecraft attitude uses quaternions.

5.2.1 Three-Component Representation

The three-component representation uses three parameters to represent the rotations, so this is the easy way to view the representations for filtering. But three-component representation requires a lot of computing power because this representation needs a large number of trigonometric functions.

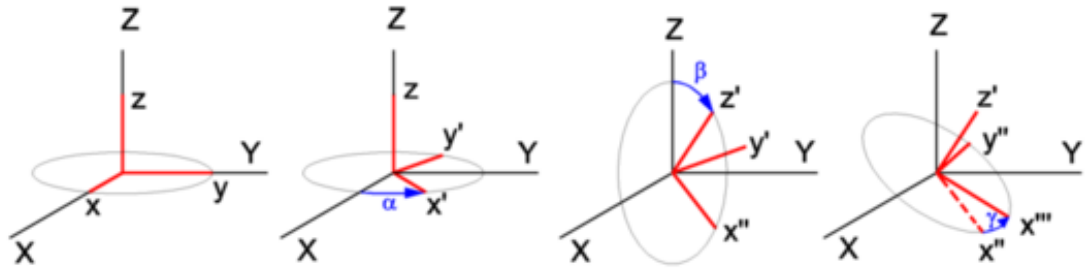

Figure 5.1: Proper Euler Angles
Source: http://www.tau.ac.il/ tsirel/dump/Static/knowino.org/wiki/Euler$_{a}ngles.html$

where, see figure 5.1, α is the rotation around the z axis, β is the rotation around the y' axis and γ is the rotation around the z' axis.

5.2.2 Adaptive Quaternion Representation

The quaternion option for the representation of spacecraft attitude is a good option because quaternions does not have singularities, but do they need to satisfy some normalization.

Adaptive quaternion is the true quaternion (denoted by q^{true}), which is the sum of the estimated quaternion (denoted by $\hat{q}$) with the error quaternion (denote by Δq),

$$q^{true} = \Delta q + \hat{q} \tag{5.3}$$

In this representation, one need to be carefull with the implementation of the extended Kalman filter, EKF, because in the update equation there is normalization problem [13],

$$\hat{q}^{+} = \hat{q}^{-} + K[y - h(\hat{x}^{-})] \tag{5.4}$$

5.2.3 Multiplicative Quaternion Representations

The multiplicative quaternion representation, as the name implies, the true quaternion is the product between the error quaternion and the estimate quaternion.

$$q^{true} = \Delta q \otimes \hat{q} \tag{5.5}$$

For the spacecraft attitude estimation in this dissertation we will used the multiplicative extended Kalman filter, MEKF, where the "global" attitude representation is the quaternion and as the "local" attitude representation is the three-component state vector, denoted by $\delta\vartheta$.

In comparison between the adaptive quaternion with the multiplicative quaternion, the multiplicative quaternion does not uses so much computational power. Using this quaternion representation one can make a single vector measurement every time [13].

5.3 Attitude Estimation

This Section presents the extended Kalman Filter and Murrell's version to estimate the spacecraft attitude. On both methods the attitude estimation is calculated sequentially.

5.3.1 Extended Kalman Filter

The extended kalman filter estimate the spacecraft attitude but for estimate attitude of the spacecraft we need also estimate the angular velocity, denoted by ω of the spacecraft. From Euler's equation of inverse kinematics, the angular velocity one get,

$$\omega = \begin{bmatrix} \cos\theta\cos\psi & \sin\psi & 0 \\ -\cos\theta\sin\psi & \cos\psi & 0 \\ \sin\theta & 0 & 1 \end{bmatrix} \begin{bmatrix} \dot{\phi} \\ \dot{\theta} \\ \dot{\psi} \end{bmatrix} \tag{5.6}$$

The quaternions kinematics model is given by,

$$\dot{q} = \frac{1}{2}\Xi(q)\omega = \frac{1}{2}\Omega(\omega)q \tag{5.7}$$

where

$$\Omega(\omega) = \begin{bmatrix} -[\omega\times] & \omega \\ -\omega^T & 0 \end{bmatrix} \tag{5.8}$$

The Kalman filter is made by three-step iterations: measurement update, state vector reset and propagation to the next measurement time [13]. The first step renovate the error state vector. The second step resets the components of the error state to zero. The last step propagates the others

variables to the next iteration [13].

Table 5.2 shows the algorithm, to initialize the extended Kalman filter with initial quaternion, the bias initial condition is considered null and it is constant along the time. The error convariance matrix, denoted by P, the first three diagonal elements are the attitude errors. Next, to calculate the gain (denoted by K) it is necessary the sensitivity matrix (denoted by H), measurement error covariance (denoted by R) and the error convariance matrix. Now, the error convariance matrix, error-state (denoted by $\Delta\hat{x}_k^+$, bias and the quaternion are update. Note in update step the quaternion is re-normalized. Lastly, in propagation the estimation of angular velocity is calculated and it is substituted in the quaternion kinematics model, see equation (5.3). Also the the error covariance matrix is propagated to the next observation [13].

Table 5.2: Extended Kalman Filter for attitude estimation.

Initialize	$\hat{q}(t_0) = \hat{q}_0, \hat{\beta}(t_0) = \hat{\beta}_0, P(t_0) = P_0$
Gain	$K_k = P_k^- H_k^T(\hat{x}_k^-)\left[H_k(\hat{x}_k^-)P_k^- H_k^T(\hat{x}_k^-) + R_k\right]^{-1}$
	$H_k(\hat{x}_k^-) = \begin{bmatrix} [A(\hat{q}^-)r_1\times] & 0_{3*3} \\ \vdots & \vdots \\ [A(\hat{q}^-)r_N\times] & 0_{3*3} \end{bmatrix}$
Update	$P_k^+ = \left[I - K_k H_k(\hat{x_k}^-)\right] P_k^-$
	$\Delta\hat{x}_k^+ = K_k\left[y_k - h_k(\hat{x}_k^-)\right]$
	$\Delta\hat{x}_k^+ \equiv \begin{bmatrix} \delta\hat{\vartheta}_k^{+T} & \delta\hat{\beta}_k^{+T} \end{bmatrix}^T$
	$h_k(\hat{x}_k^-) = \begin{bmatrix} A(\hat{q}^-)r_1 \\ A(\hat{q}^-)r_2 \\ \vdots \\ A(\hat{q}^-)r_N \end{bmatrix}$
	$\hat{q}^* = \hat{q}_k^- + \frac{1}{2}\Xi\hat{q}^-\hat{\vartheta}_k^+$
	$\hat{q}^+ = q^*/\|q^*\|$
	$\hat{\beta}_k^+ = \hat{\beta}_k^- + \Delta\hat{\beta}_k^+$
Propagation	$\hat{\omega}(t) = \hat{\omega}(t) - \hat{\beta}(t)$
	$\dot{\hat{q}}(t) = \frac{1}{2}\Xi()\hat{q}(t))\hat{\omega}(t)$
	$\dot{P}(t) = F(t)P(t) + P(t)F^T(t) + G(t)Q(t)G^T(t)$

5.3.2 Murrell's version

The advantage of the Murrell's version in relation to the extended Kalman filter, EKF, is that the Murrell's version requres less computation power when because it does not need to invert 3×3 matrix to calculate the gain.

To avoid to invert a 3×3 matrix, Murrell's version process each time a 3×1 vector and waits to all complete observation. The N is the number of observations that the this method need to have to compute the gain [13].

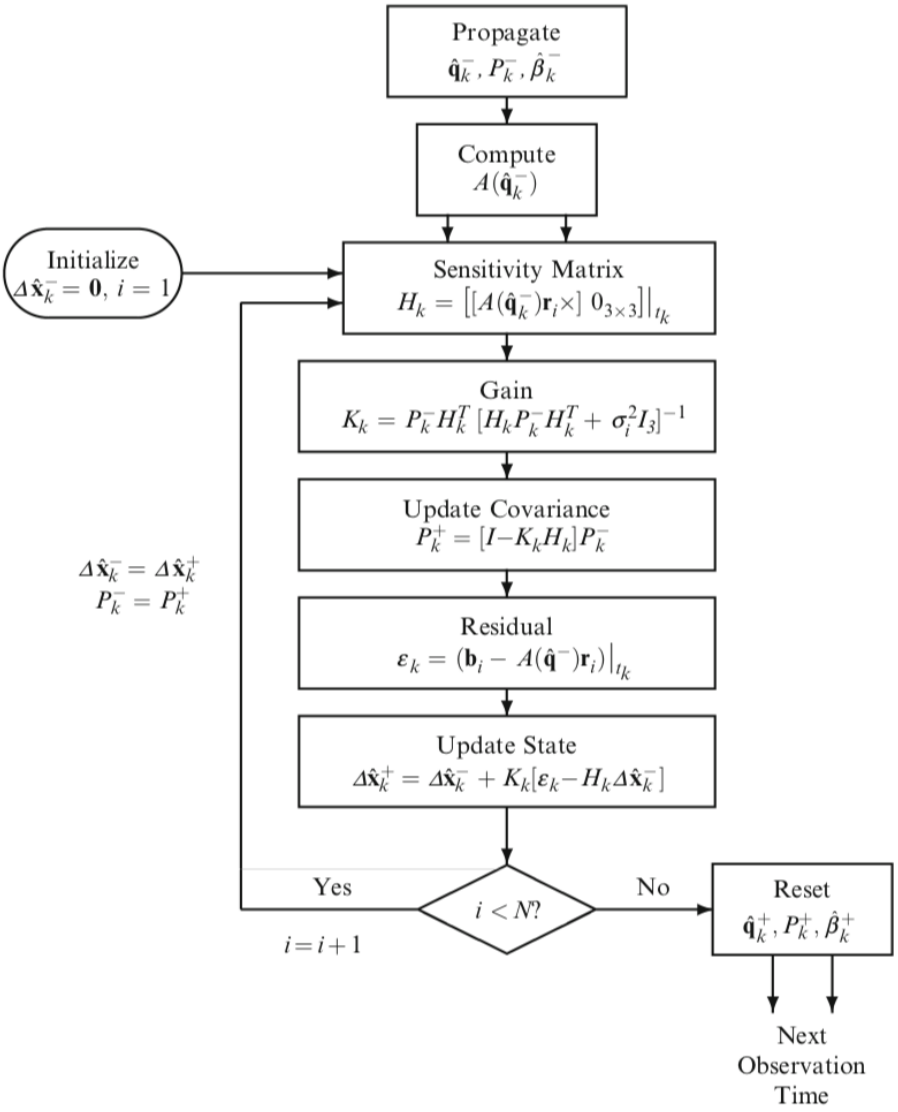

Figure 5.2: Computationally efficient attitude estimation algorithm.
Source: [13]

Figure 5.2, shows the estimated method Murrell's version that begins the same way as the extended kalman filter, with the propagation of initial quaternion, gyro bias and error covariance. Next, the attitude matrix is computed and then with a vector the state and the error covariance are updated. Next all the step is the same as the extended kalman filter. This cycle is finished when all vector observations are concluded. The last step the error covariance, global state and global state are propagate to the next time [13].

5.4 Simulation Results

This Section illustrates through computer simulations the attitude estimation of a spacecraft. The estimator was implemented in Matlab software tool.
First it will be demonstrated the quaternions error between the desired attitude and the actual attitude and then the quaternions errors with different noise parameters.

The initial parameters for extended Kalman filter are: initial bias for each axis was set to 0.1 rad/s, the initial covariance was set to 0.2 rad/s and the initial quaternions for attitude was $q_0 = [1;0;0;1]$. The desired quaternions for this simulation was $q_d = [0;0;0;1]$. The noise parameters for gyro measurements are set $\sigma_u = \sqrt{10} \times 10^{-15}\ rad/s^{3/2}$ and $\sigma_v = \sqrt{10} \times 10^{-7}\ rad/s^{1/2}$.

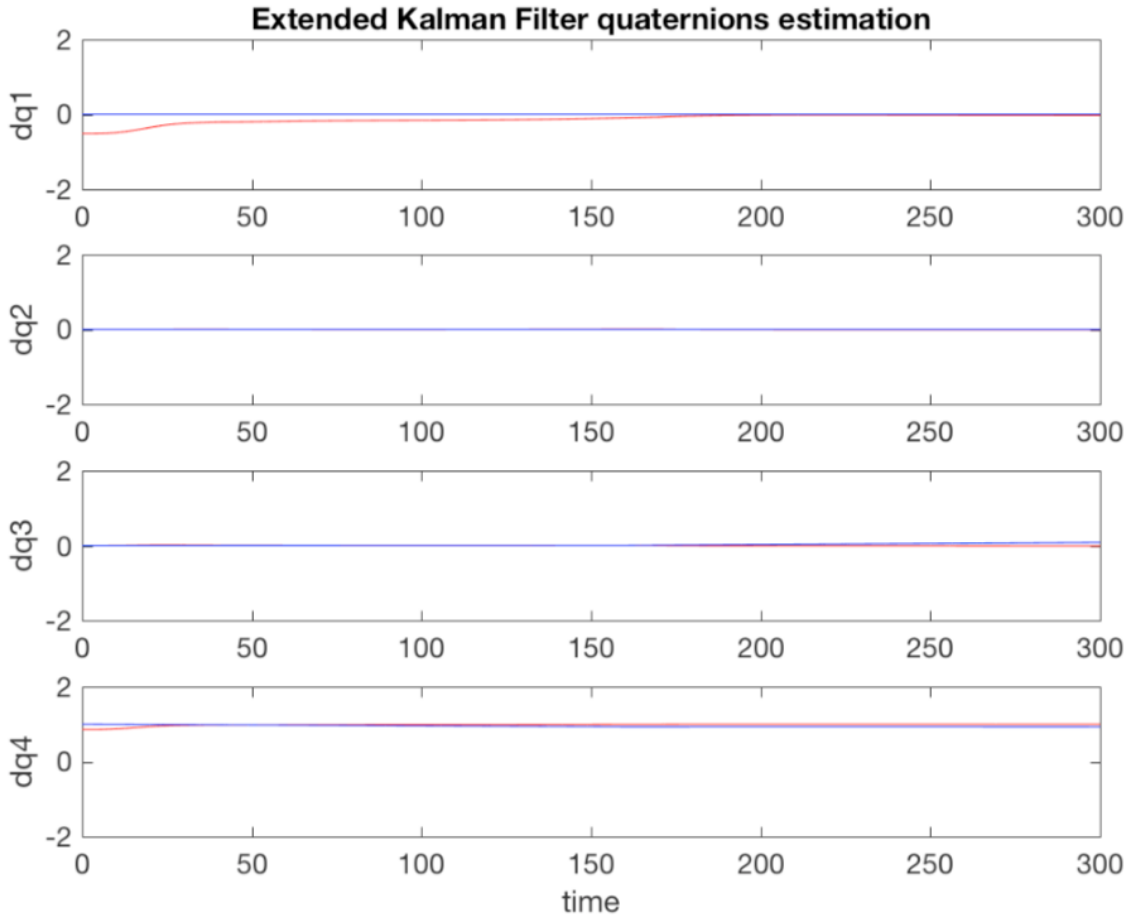

Figure 5.3: Estimator Extended Kalman Filter Quaternions Errors.

Figure 5.3 displays in red the quaternions error and in blue the desired quaternions. The quaternions error is the difference between the estimated quaternions and the true quaternions. Note that the forth error goes close to one when the first three error quaternions are near zero.

The following figures present the results of the quaternions error for different noise parameters. We changed the σ_u for gyro measurements to $\sigma_u = \sqrt{10} \times 10^{-20}\ rad/s^{3/2}$ (see figure 5.4), $\sigma_u = \sqrt{10} \times 10^{-2}\ rad/s^{3/2}$ (see figure 5.5).

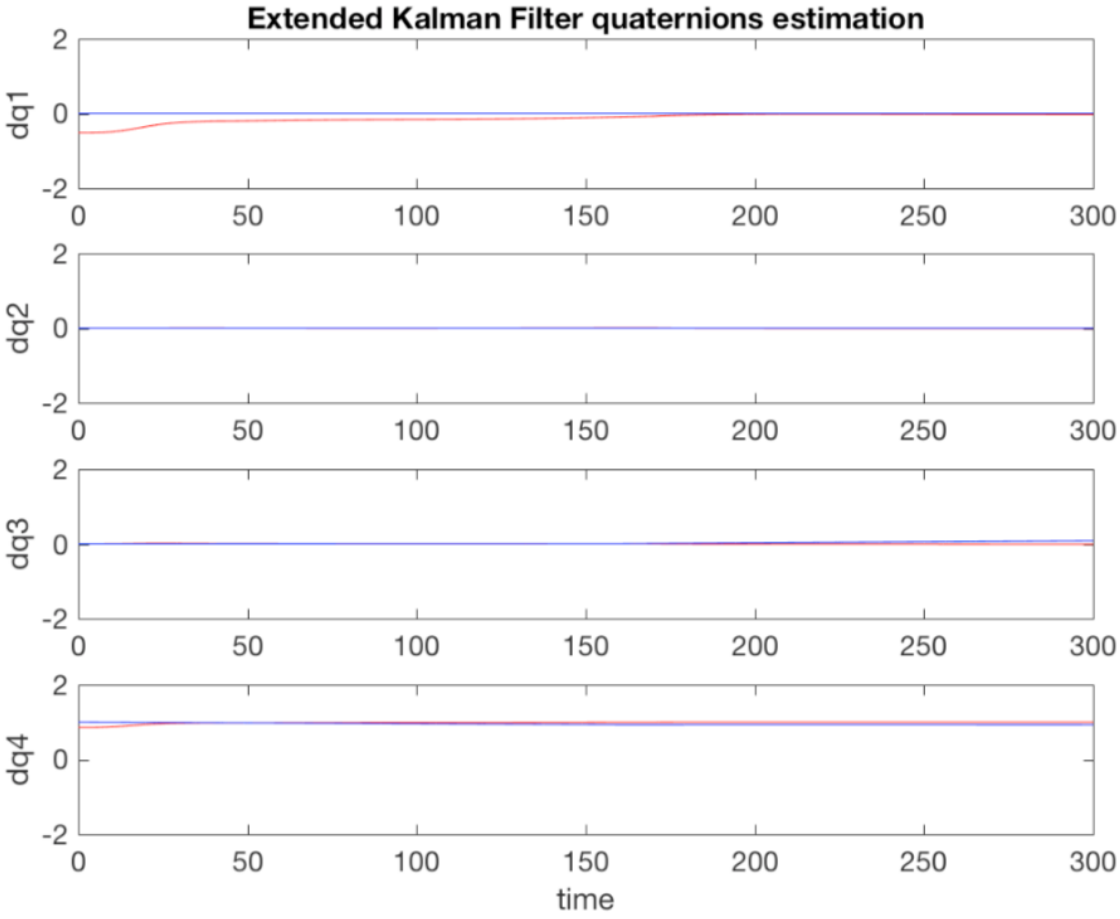

Figure 5.4: Estimator Extended Kalman Filter Quaternions Errors.

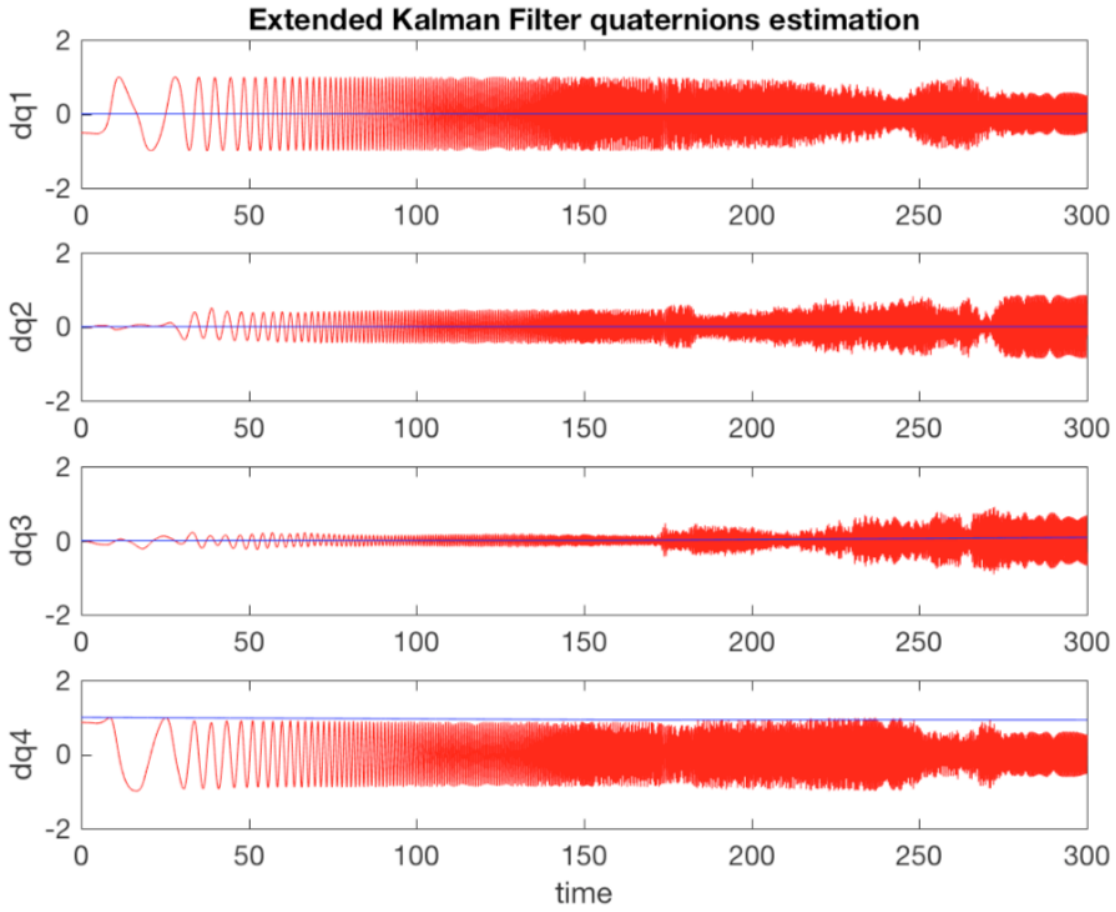

Figure 5.5: Estimator Extended Kalman Filter Quaternions Errors.

Figure 5.5 shows a case that the filter do not converge, where the noise parameters for gyro measurements is $\sigma_u = \sqrt{10} \times 10^{-2}\ rad/s^{3/2}$ which is too much. In figure 5.4, the noise is $\sigma_v = \sqrt{10} \times 10^{-20}\ rad/s^{3/2}$ and we can already see that the quaternions errors goes to near zero.

Chapter 6

Attitude Control

This chapter describes the attitude control of a spacecraft. The attitude control is fundamental to provide the adequate control signals to the actuators to change the actual locations to a desired attitude. When the spacecraft has a fixed and desired location, the angular velocity of the actuators, reaction wheels, will be zero. Section 6.1 provide a brief review of state models and the negative feedback control diagram. We will focus on the dynamic's model because our model for a spacecraft is a dynamic model. In Section 6.2 we will present the single axis attitude control system, and in particular the proportional-derivative controller the closed-loop dynamics. Also in this Section we will show the Lyapunov's method to prove that the nonlinear system is stable. Section 6.3 will particularize the attitude control for reaction wheels. Lastly, in Section 6.4 we illustrate through computer the simulations controller used to move the spacecraft to a target desired attitude.

6.1 Control background

This Section presents simple results on nonlinear and linear control. The system can be continous-time or discrete-time. To study a system it is necessary to understand its behaviour and to this effect that we need to model the system. The model can be static or dynamic. A static model is invariant to time. On the other hand, a dynamic model depends of time, and usually on the past state.

6.1.1 State Models

The ordinary discrete-time linear state space representation is given by,

$$x_{k+1} = A_k x_k + B_k u_k \tag{6.1}$$

$$y_k = C_k x_k + D_k u_k \tag{6.2}$$

where, x_k denotes a state vector, u is the input vector and the output vector is denoted by y_k.

The state transition matrix allows to relate solution from two instants of time. The properties of discrete-time state transition matrix (denoted by $\Phi_{(k,k)}$) are:

$$\Phi_{(k,k)} = I$$

$$x_k = \Phi_{(k,0)} x_0$$

$$\Phi_{(k+1,l)} = A_k \Phi_{(k,l)}$$

6.1.2 Control Theory

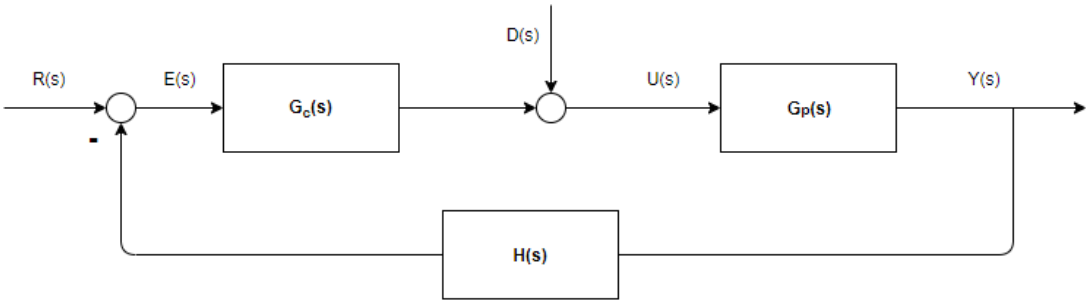

Figure 6.1: Negative feedback control block diagram.

Figure 6.1 describes a typical negative feedback control diagram for the continuous time case, where $R(s)$ is the reference, $Y(s)$ is the output, the error is denoted by $E(s)$, $G_c(s)$ is the controller, the disturbance is represent by $D(s)$, $U(s)$ is the control input, $G_p(s)$ is the plant to be controlled and $H(S)$ is the sensor dynamics.

In order to verify if the closed-loop system is asymptotically stable all of the roots must be in the left of the imaginary axis.

The transfer function between the output and the reference consider the disturbance is null, is given by,

$$\frac{Y(s)}{R(s)} = \frac{G_c(s)G_p(s)}{1 + G_c(s)G_p(s)H(s)} \tag{6.3}$$

Now, if consider reference null, the transfer function between the output and disturbance one get,

$$\frac{Y(s)}{D(s)} = \frac{G_p(s)}{1 + G_c(s)G_p(s)H(s)} \tag{6.4}$$

6.2 Single Axis Attitude Control

This Section presents the single axis attitude control system.

By applying the Euler's rotational equations of motion to single axis one get,

$$J\ddot{\theta} = u \tag{6.5}$$

where, the inertia of the spacecraft is denoted by J, θ is the angle and u is the torque applied of spacecraft.

For a Proportional-Derivative (PD) controller the closed-loop dynamics are given by,

$$\frac{Y(s)}{U(s)} = \frac{G_c}{Js^2 + k_d s + k_p} \tag{6.6}$$

where, k_p is the proportional gain, k_d is the derivative gain relate to the derivative part of the controller, a the G_c is given by

$$G_c = k_d s + k_p \tag{6.7}$$

6.2.1 Stability of Nonlinear Dynamic Systems

To prove that a nonlinear system is stable it is more challenging that for linear system. The problem of stability of a nonlinear system can be in some case be resolved by applying one of the two methods of Lyapunov: *Lyapunov's linearization method* and *Lyapunov's direct method*.

To this end, we need to introduce the notion of an equilibrium point, denoted by x_e. An equilibrium point is defined as the point that if the system starts at that point, then it stays on it for all time, which implies that, $\dot{x}(t) = 0$ along the time.

The Lyapunov's linearization method could be a good approach to determine if a system is locally stable but the system needs to be within a linear region.

The stability conditions of Lyapunov's linearization method are [7]:

- The equilibrium point is asymptotically stable if all eigenvalues of F (Jacobian of f(x)) are strictly in the left-half complex plane.

- The equilibrium point is unstable if at least one eigenvalue is strictly on the right-hand complex plane.

- Stability cannot be concluded if there exists at least one eigenvalue of F on the jw axis (imaginary axis) and the others are in the left-half complex plan..

The Lyapunov's direct method is an effective method for analyse the stability of the nonlinear and linear systems. This method uses a scalar function, $V(x)$, that needs be continuous and has continuous derivatives.

The conditions of Lyapunov's direct method for chosen the scalar function, $V(x)$, are (assuming that $x_e = 0$):

- $V(x_0) = 0$,
- $V(x) > 0$ for x $\neq x_0$
- $\dot{V}(x) < 0$

The scalar function needs verify all previously conditions to be a Lyapunov function.

- The system is asymptotically stable if $\dot{V}(x) < 0$ for $x \neq x_0$.

- The system is stable if $\dot{V}(x) \leq 0$ (LaSalle's theorem to prove assimptotically).

6.3 Attitude Control: Reaction Wheels

The relations between the attitude of the spacecraft and the angular velocity are given by Euler's rotational equation of motion and the attitude kinematics.

The quaternion attitude kinematics is given by,

$$\dot{q} = \frac{1}{2}\Xi(q)\omega = \frac{1}{2}\Omega(\omega)q \tag{6.8}$$

and the Euler's rotation equation of motion as

$$J\dot{\omega} = -[\omega\times]J\omega + L \tag{6.9}$$

For the reaction-wheel the Euler's rotational equation is particularized to

$$J\dot{\omega} = -[\omega\times](J\omega + h) + \tau \tag{6.10}$$

where, J is the inertia of the wheels, h is the wheel angular moment ($h \equiv H^w$) and τ is the wheel torque.

The total angular momentum, denoted by H, is conserved and one get,

$$H = J\omega + h \tag{6.11}$$

The reaction-wheel the Euler's rotation equation is usually given by,

$$J\dot{\omega} = -[\omega\times]J\omega + \bar{L} \tag{6.12}$$

and

$$\tau = -[\omega\times]h - \bar{L} \tag{6.13}$$

where, $\bar{L}$ is the actual wheel torque input.

For the wheel torques the linear control law one get,

$$\bar{L} = -k_p sign(\delta q_4)\delta q_{1:3} - k_d\omega \tag{6.14}$$

and the nonlinear control law is given by,

$$\bar{L} = -k_p sign(\delta q_4)\delta q_{1:3} - k_d(1 - \delta q_{1:3}^T q_{1:3})\omega \tag{6.15}$$

where k_p is the proportional gain and the derivative gain denoted by k_d.

Using the Lyapunov function it is possible show that the linear and nonlinear control laws are asymptotic stable [12]. In the book [12] we can see more in detail the linear and nonlinear control laws for the wheel torque.

6.3.1 Lyapunov's Direct Method

To prove that the closed loop system is stable we will apply the Lyapunov's second method.

Using the multiplicative quaternions, the quaternions errors is given by,

$$\delta q \equiv \begin{bmatrix} \delta q_{1:3} \\ \delta q_4 \end{bmatrix} = q \otimes q_c^{-1} \tag{6.16}$$

where,

$$\delta q_{1:3} = \Xi^T(q_c)q \tag{6.17}$$

and

$$\delta q_4 = q^T q_c \tag{6.18}$$

Using as Lyapunov candidate function, denoted by V is given by,

$$V = \frac{1}{4}\omega^T J\omega + \frac{1}{2}k_p \delta q_{1:3}^T \delta q_{1:3} + \frac{1}{2}k_p(1-q_4)^2 \geq 0 \tag{6.19}$$

The time derivative of Lyapunov function yields,

$$\dot{V} = -\frac{1}{2}(\omega^T \delta q_{1:3})[k_p + k_p \delta q_4 - k_p(1+\delta q_4)] - \frac{1}{2}k_d \omega^T \omega = -\frac{1}{2}k_d \omega^T \omega \leq 0 \tag{6.20}$$

Since $\dot{V} \leq 0$ the closed-loop system is stable.

LaSalle's theorem is then used to prove asymptotic stability. For that, we need to specify an invariant set. Note that G is an invariant set if the system trajectory stars from a point G it will stay in G for all the time.

Consider that $\dot{V}(x) \leq 0$ is true in all state space and that $V(x) \to \infty$ just as $\| x \| \to \infty$. Let E be the set of all points in $\dot{V}(x) = 0$ and M be the largest invariant set in E. Therefore, LaSalle's theorem states that all solutions globally asymptomatically converge to M as time goes to infinity.

6.4 Simulation Results

In this section, we illustrate through computer simulations the behaviour of the proposed attitude controller.

In the implementation, we used the satellite Sentinel-2 as a model, which has a mass of 1200 Kg and a the moment of inertia is given by

$$I = \begin{bmatrix} 1321.94 & 0 & 0 \\ 0 & 2205.46 & 0 \\ 0 & 0 & 1414.9 \end{bmatrix} \tag{6.21}$$

In this simulation, the desired quaternion of the spacecraft was set to $q = [0;0;0;1]$ and the initial quaternion was set to $q_0 = [1;0;0;0]$. The gains of the controller were set to $k_p = 50$ and $k_d = 500$. The defined maximum speed of the reactions wheels was 0.05 rad/s.

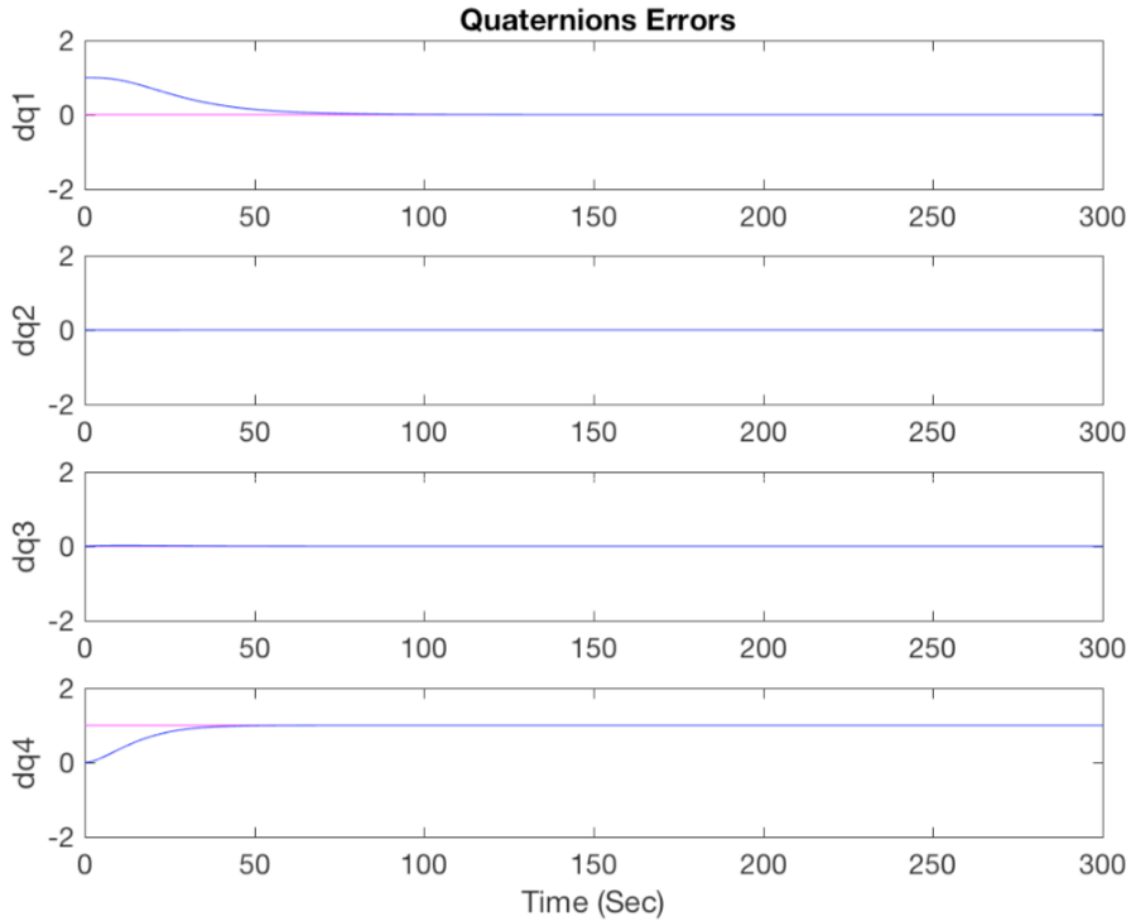

Figure 6.2: Controller quaternions.

Figure 6.2 shows the quaternions state along the time and the desired quaternions. Note that actuators are activated by the controller when the attitude of the spacecraft is different of the desired attitude.

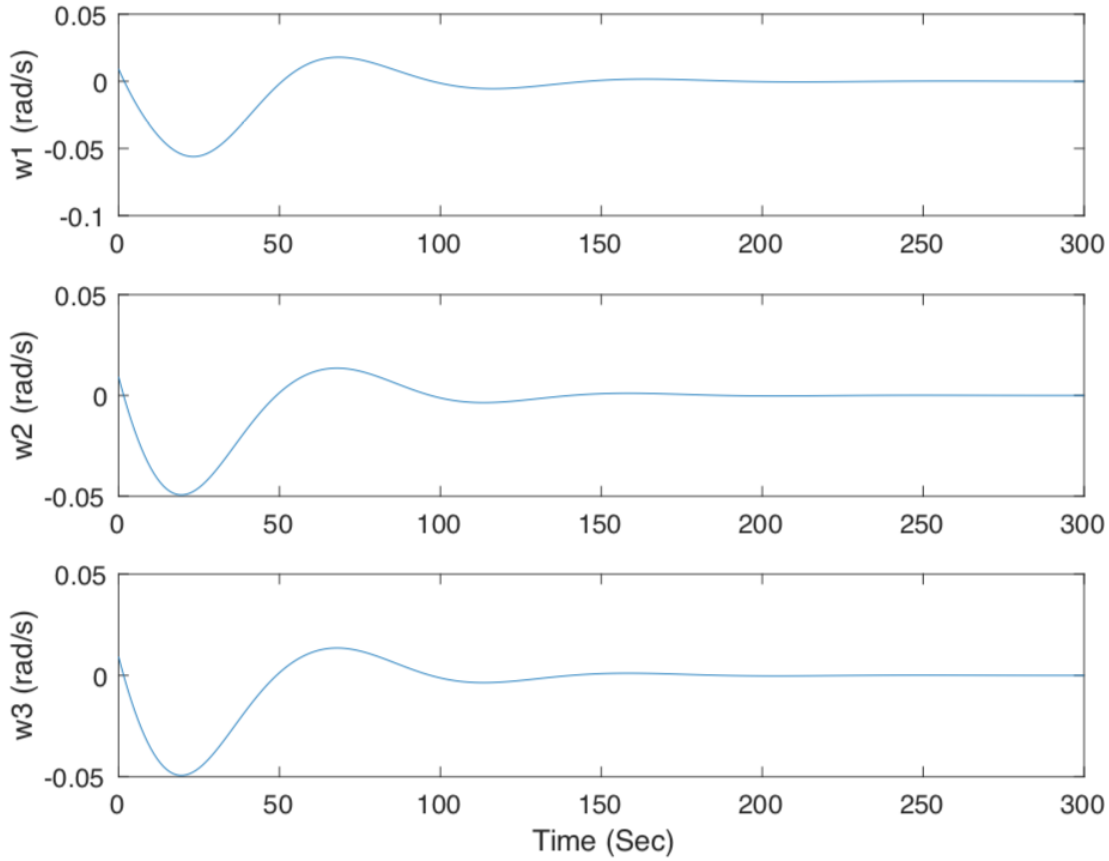

Figure 6.3: Angular velocity of reaction wheels.

Figure 6.3, displays the angular velocity of the actuators reactions wheels reaches the maximum speed when the quaternions error is greater and angular velocity starts to accelerate slowly when the desired quaternions are close to achieving. The reactions wheels stops acting when the desired attitude is reached.

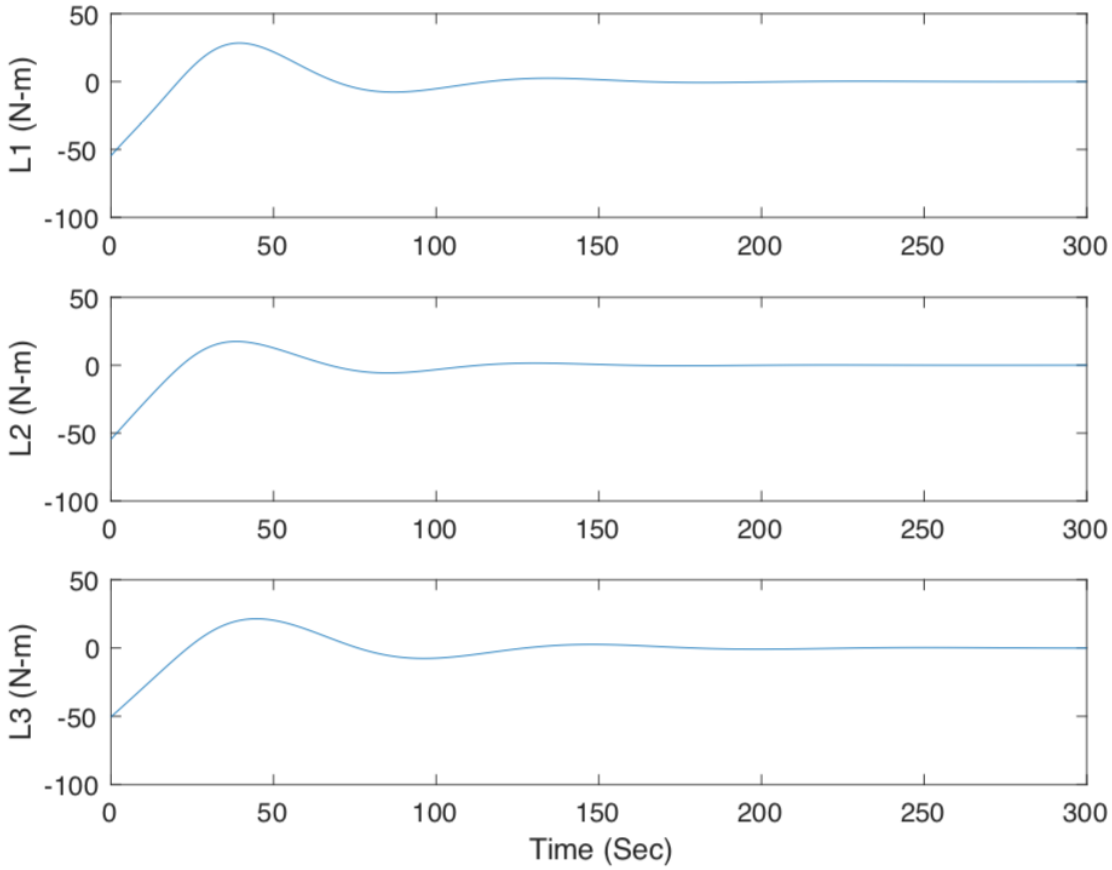

Figure 6.4: Torque of reaction wheels.

Figure 6.4, displays the moment of the wheel and it shows that the momentum reaches its maximum when the error is greater and it begins to decrease approximately in the 50 seconds when the desired quaternions is accomplished.

Following we present the simulations for the nonlinear control. This simulation was the same parameters as the linear control simulation of this chapter.

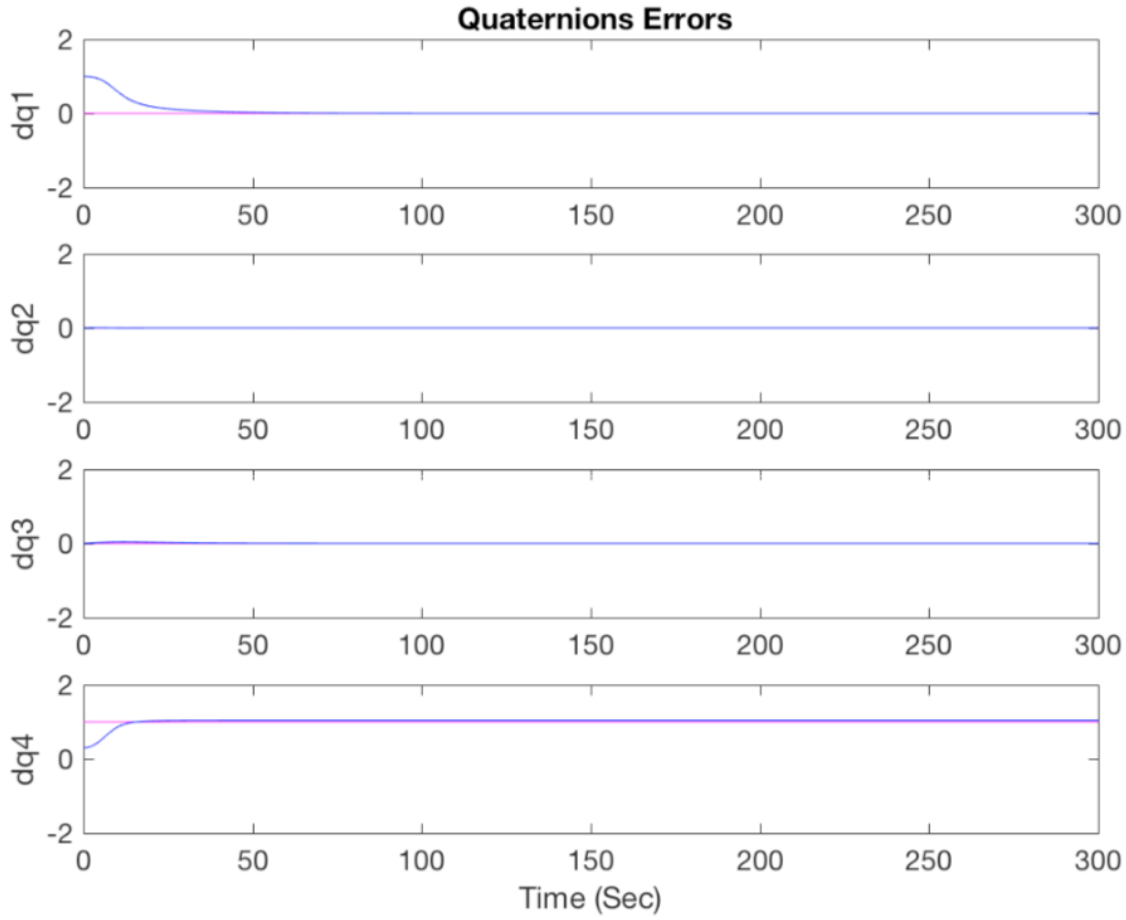

Figure 6.5: Nonlinear control law.

The nonlinear control (see figure 6.5) has a shorter rise time in comparison with linear control (see figure 6.2).

In the following we present the simulations for the results in blue the quaternions error for different proportional gain of the controller and in red the desired quaternions. We changed the proportional gain to the $k_p = 10$, $k_p = 30$ and $k_p = 200$ see figures 6.6, 6.7 and 6.8.

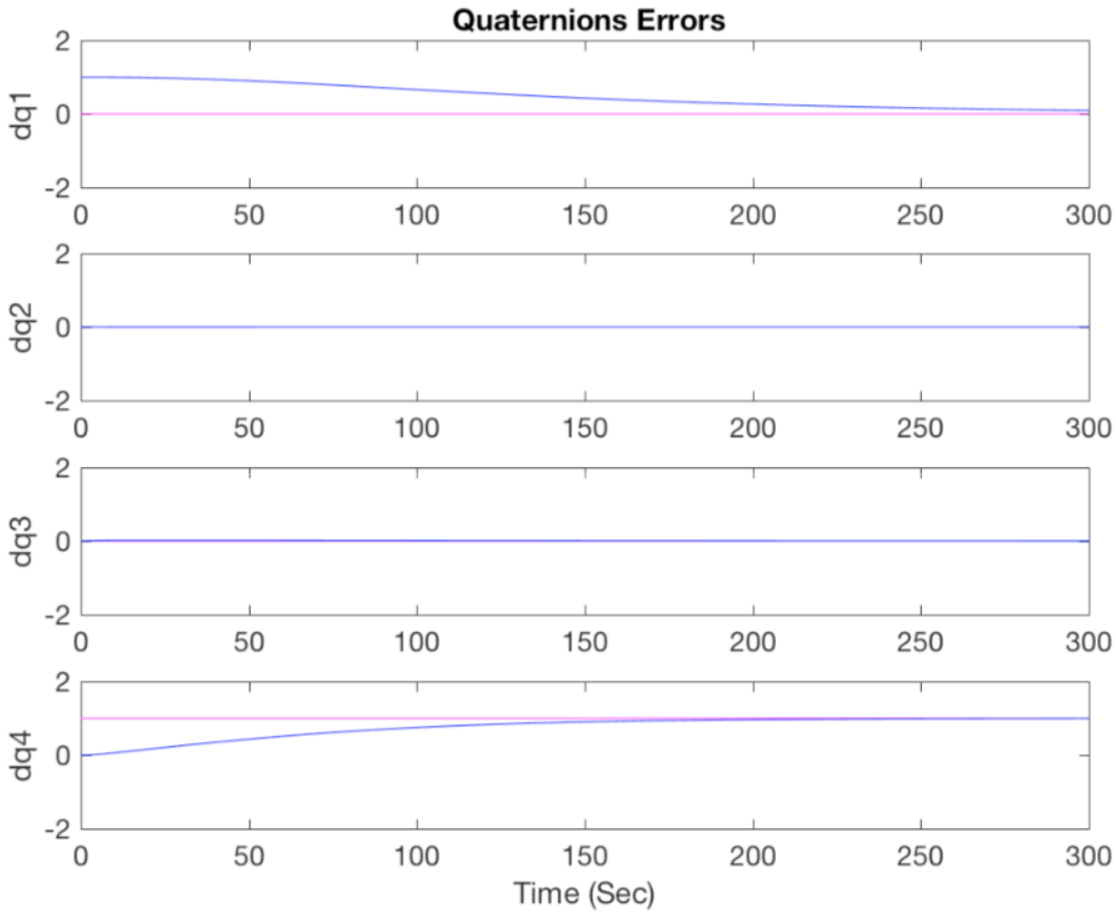

Figure 6.6: Controller quaternions erros with $k_p = 10$.

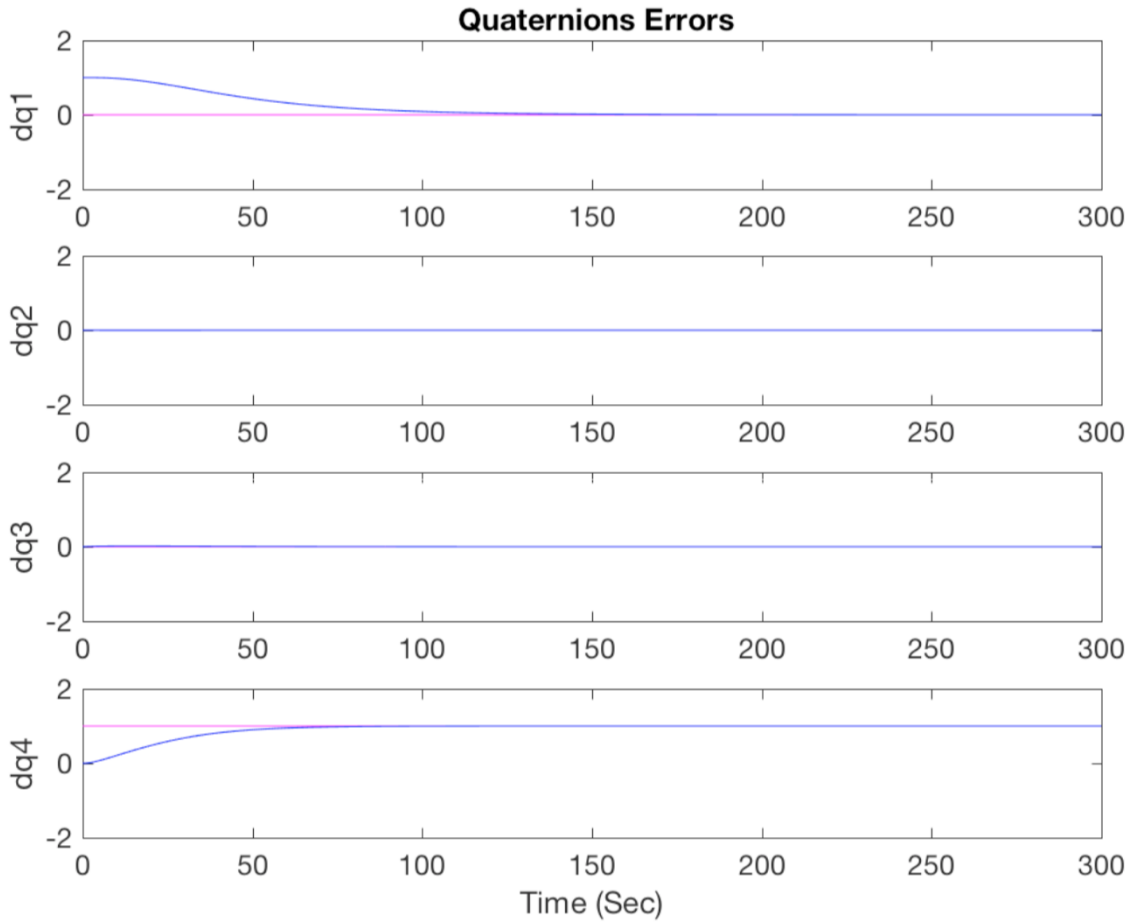

Figure 6.7: Controller quaternions erros with $k_p = 30$.

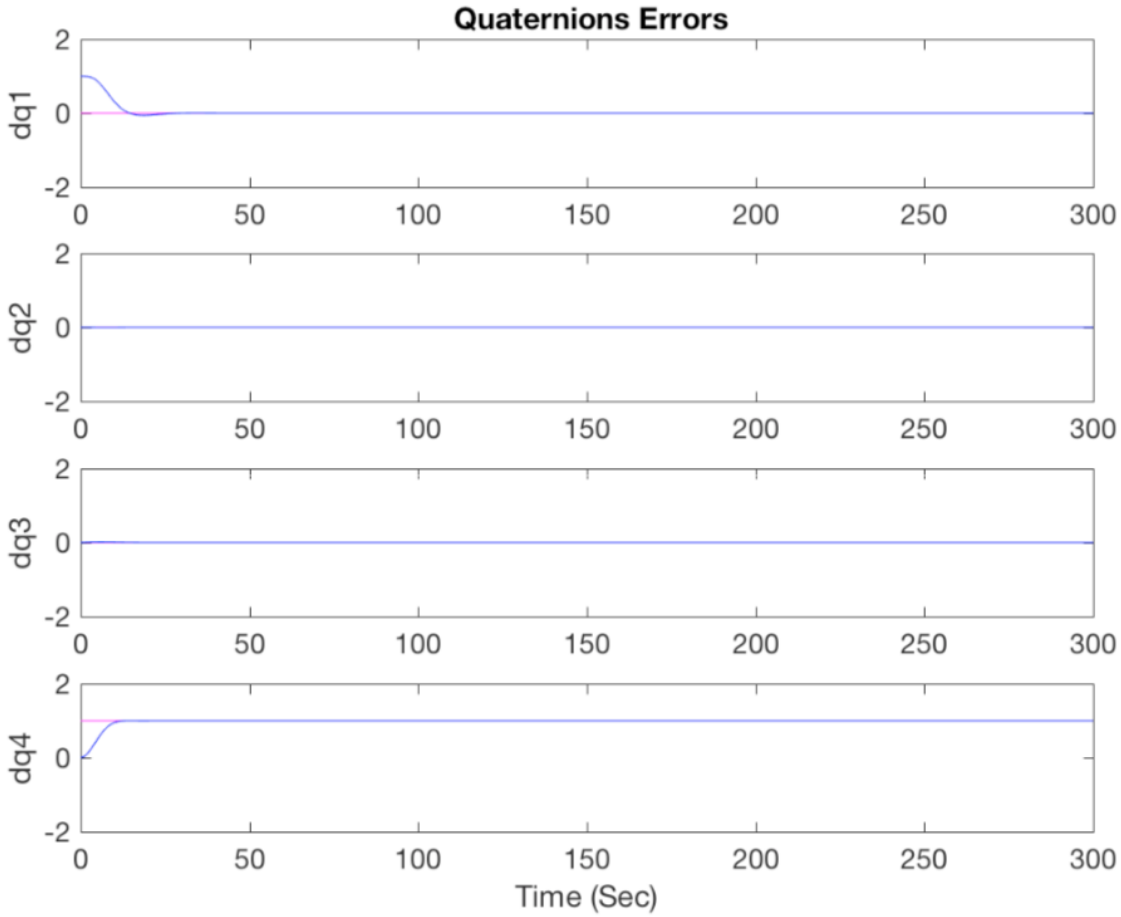

Figure 6.8: Controller quaternions erros with $k_p = 200$.

We can conclude that the lower proportional gain is, the greater the time will be for the the quaternions errors to go to zero.

On next, it is displayed in blue the quaternions error for different derivative gain of the controller and in red the desired quaternions. We changed the derivative gain to the $k_d = 50$, $k_d = 200$ and $k_d = 800$ see figures 6.9, 6.10 and 6.11.

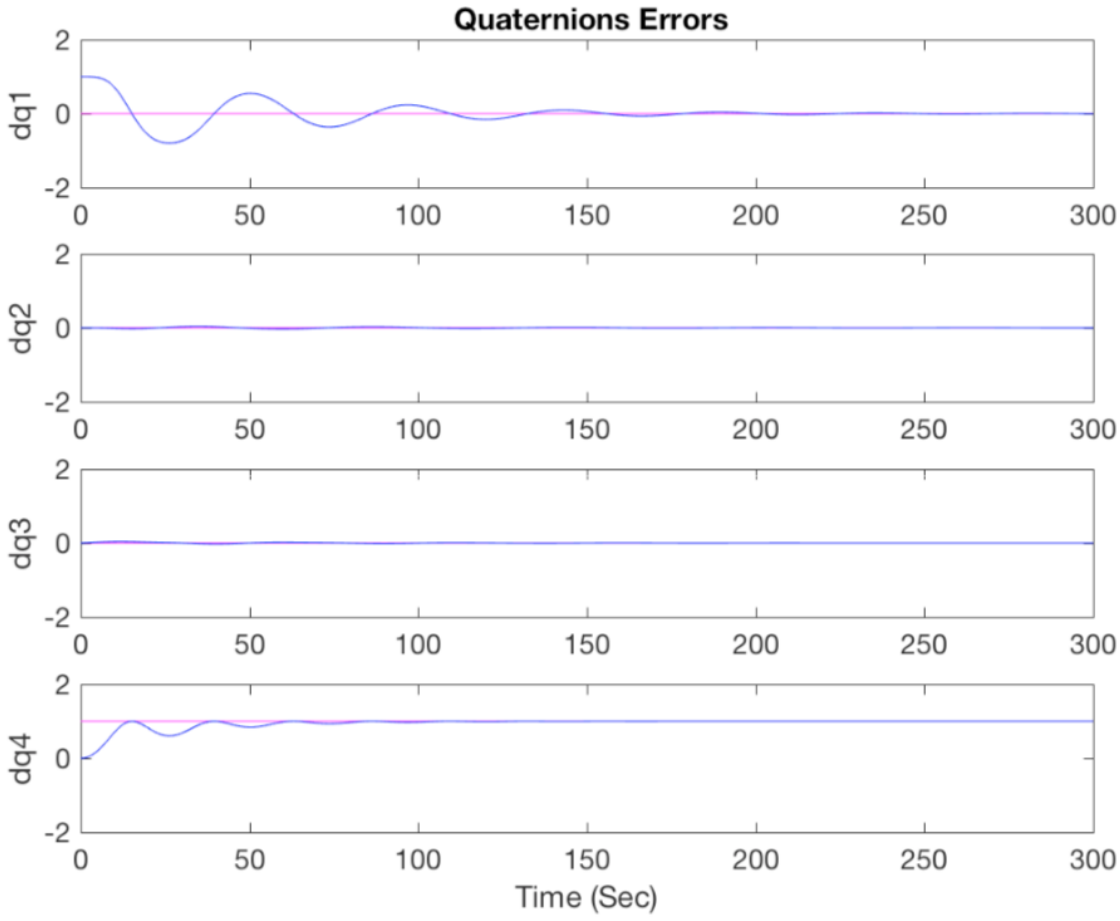

Figure 6.9: Controller quaternions erros with $k_d = 50$.

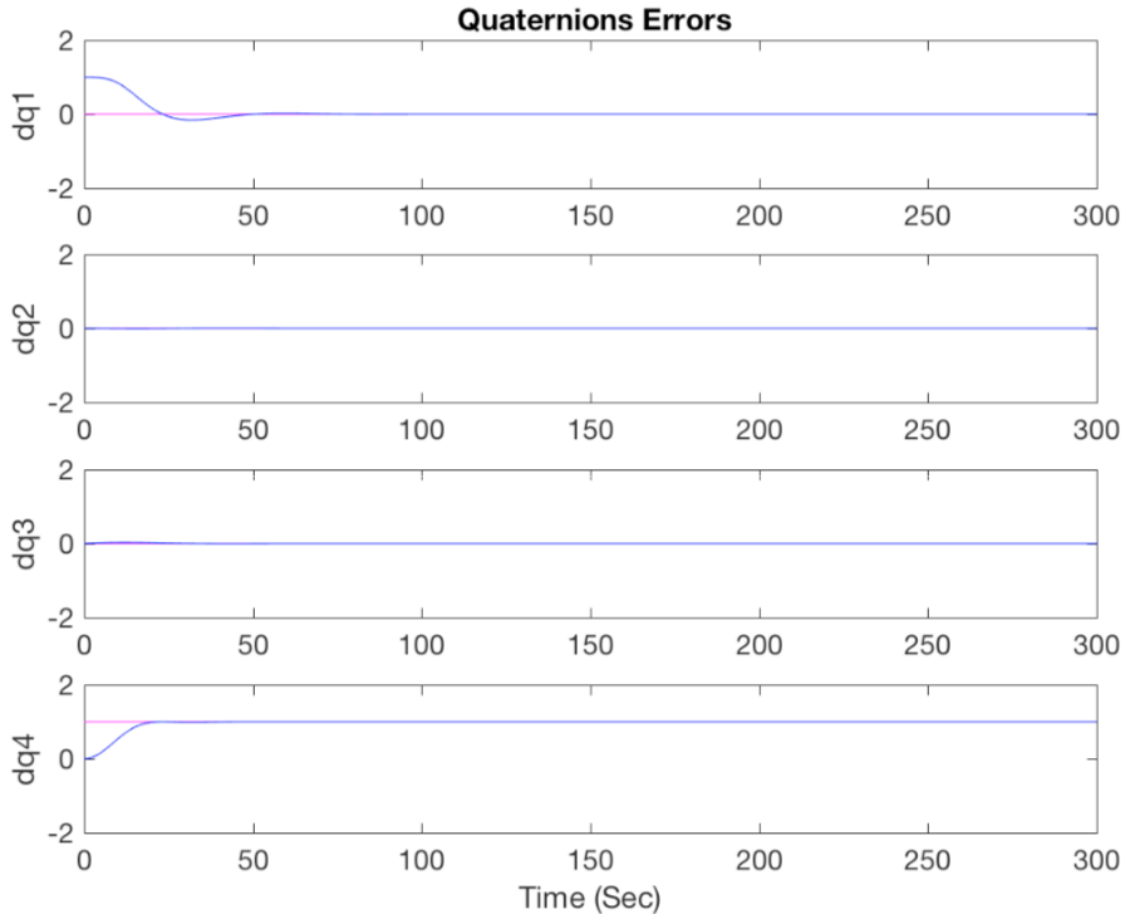

Figure 6.10: Controller quaternions erros with $k_d = 200$.

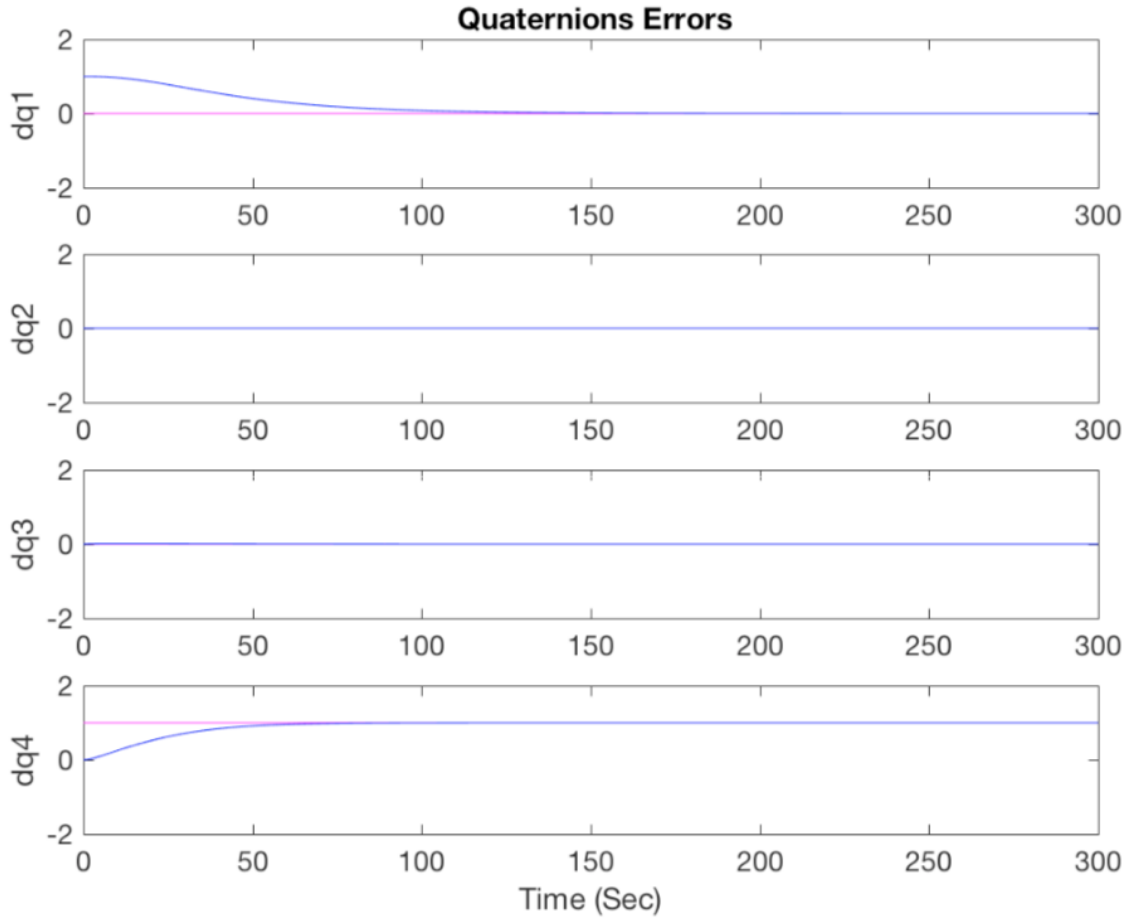

Figure 6.11: Controller quaternions erros with $k_d = 800$.

As we can observe, we concluded that with smaller derivative gain quaternions errors we get more oscillation because the proportional gain is bigger. If the gain is big enough, there will be no oscillations. Thus, the bigger proportional gain is, the faster the response of our system is and big derivative gains leads to smaller percentage overshoot. Figure 6.6, we can see that the proportional gain is smaller and consequently the time response of our system is slower.

Chapter 7

Space Rendezvous

This chapter is dedicated to the rendezvous orbital dynamics and control (RODC).
Section 7.1 provides a brief review of the phases of space rendezvous. Section 7.2 is dedicated to the linear relative dynamics. Section 7.3 shows the orbital maneuver to change the orbit of a spacecraft. Lastly, 7.4 presents the simulation results for the space rendezvous.

7.1 Space Rendezvous Background

The space rendezvous is typically two spacecrafts around the Earth where one spacecraft will approximate the target spacecraft. The spacecraft that will catch the spacecraft target needs a trajectory optimization. For that we need to define the nonlinear two-body rendezvous.

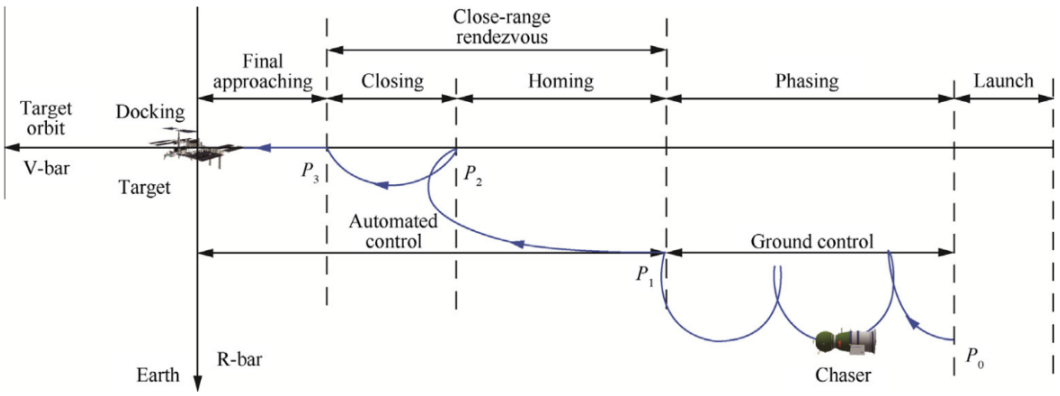

Figure 7.1: Spacecraft rendezvous process.
Source: [6]

Figure 7.1, the spacecraft rendezvous process that is composed by the following phases:

- **launch:** consists when the spacecraft is launched on Earth to orbit around the Earth;
- **phasing:** is composed by the navigation with help of some sensors of the spacecraft, for example the star tracker, to catch the target;

- **close-range rendezvous:** is composed by homing and closing phases where the chaser spacecraft is autonomous, it will obtain the target orbit and slowly reduce the relative velocity between two spacecrafts;

- **final approaching:** the spacecraft catches the target and acquires the same position, velocity and angular rate as the target;

7.2 Relative Dynamics

As we saw in the chapter 4, for the orbit control, the actuators of the spacecraft that are typically used are the thrusters as actuators of a spacecraft. In this Dissertation we will not consider the orbital perturbations.

The general linear relative dynamics in a rectangular coordinate view is given by the Clohessy-Wiltshire equations:

$$\begin{cases} \ddot{x} - 2\omega\dot{z} = a_x \\ \ddot{y} + \omega^2 y = a_y \\ \ddot{z} + 2\omega\dot{x} - 3\omega^3 z = a_z \end{cases} \tag{7.1}$$

where, a_x, a_y and a_z are the thruster acceleration components and ω is the orbital angular velocity of the target.

When the spacecraft is close to the target the origin of the coordinates system is in target's center of mass and when the distance between the two spacecrafts is considerable, the Earth is the origin of the coordinate system. The rotational dynamics of the spacecraft is already described in the Section 4.2, the Euler's equation is given by the equation (4.20). The only difference for the target is that the torque is equal to zero because it is assumed that the target is uncontrolled.

For the case when the distance between the spacecraft and target is considerable, usually in the phasing phase, the rectangular coordinates are not able to characterize the trajectory adequately so we used the Earth-centered cylindrical coordinate system [6]. In this case, the dynamics equations of the spacecraft are given by,

$$\begin{cases} \Delta\dot{r} = \Delta v_r \\ \Delta\dot{\theta} = \omega_0 \frac{\Delta r}{r_0} + \omega_0 \frac{\Delta v_t}{v_0} \\ \Delta\dot{z} = \Delta v_z \\ \Delta\dot{v}_r = \omega_0^2 \Delta r + 2\omega_0 \Delta v_t + \Delta a_r \\ \Delta\dot{v}_t = -\omega_0 \Delta v_r + \Delta a_t \\ \Delta\dot{v}_z = -\omega_0^2 \Delta z + \Delta a_z \end{cases} \tag{7.2}$$

where, mean radius is denoted by r_0, ω is the orbital angular rate and v_0 is the orbital velocity of the target. Δr, $\Delta\theta$ and Δz are the relative position, Δv_r, Δv_t and Δv_z are the relative velocity and lastly, Δa_r, Δa_t and Δa_z are the relative acceleration between the spacecraft and the target.

For more details, the work in [6] describes the dynamics equations for the different cases, such as: elliptic orbits, considering orbital perturbations, based on orbital elements differences and including second-order terms.

7.3 Rendezvous Trajectory

The phase that takes more time is the phasing phase because the spacecraft tries to obtain the target's orbit. We use the initial references of the spacecraft and the target and the main goal is to converge to the position, velocity and attitude of both spacecrafts. For that, we will use the Newton iteration method.

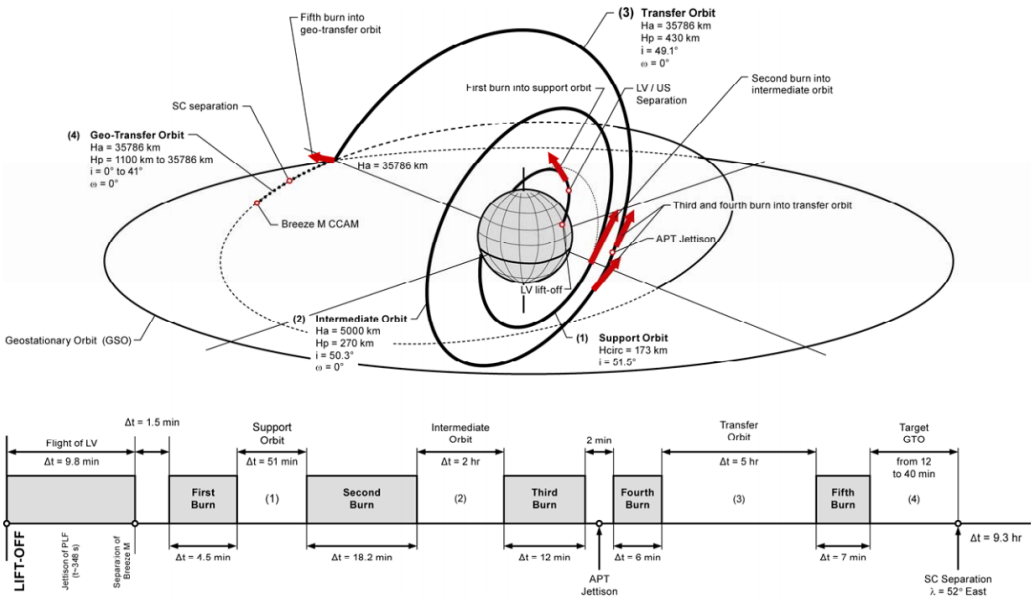

Figure 7.2: Example of burns to trajectory rendezvous.
Source: [5]

In the trajectory rendezvous it is fundamental to use the orbital maneuver (or burn) to the spacecraft in order to obtain the orbit of the target. The orbital maneuver uses the orbital-motion laws. Thus, if we want to change the spacecraft's orbit to a higher orbit we need to increase the velocity, whereas if we want to go to a smaller orbit we need to decrease the velocity by the Hohmann Transfer method. Figure 7.3 illustraste the orbital maneuver trajectory rendezvous of a spacecraft.

7.4 Simulation Results

This section presents the results about rendezvous orbital dynamics and control. The space rendezvous was implemented through computer simulations by General Mission Analyses Tool, GMAT, [84].

In this simulation we used the infinite burns configuration, that means that the fuel remains equally over time.

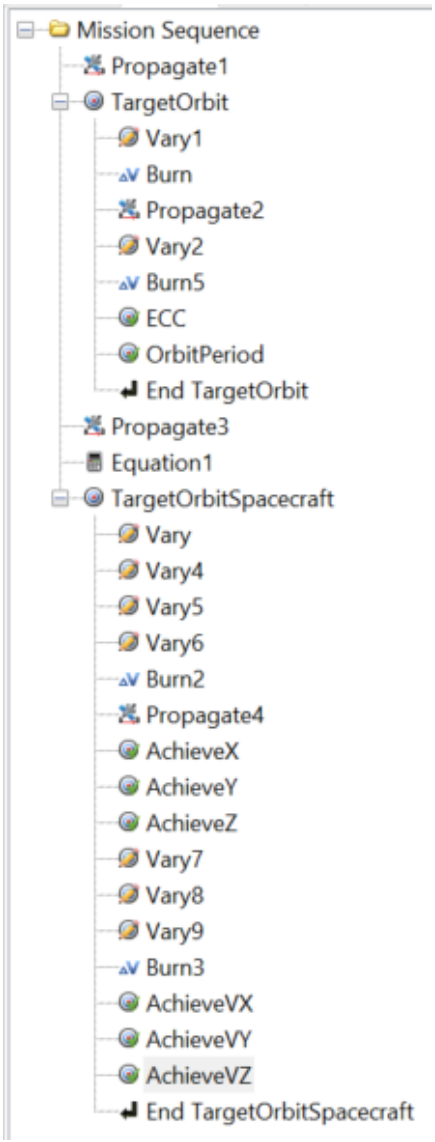

Figure 7.3: Mission sequence of the simulation.

Figure 7.3 shows the simulation mission sequence. The computer simulations starts with the launch phase, where the target moves in a orbit as the spacecraft around the Earth, correspond of Propagate1. Then, in sequence TargetOrbit, the target obtain a medium Earth orbit in the mission sequence. The sequence TargetOrbitSpacecraft is the phasing, close-range rendezvous and final approaching phases.

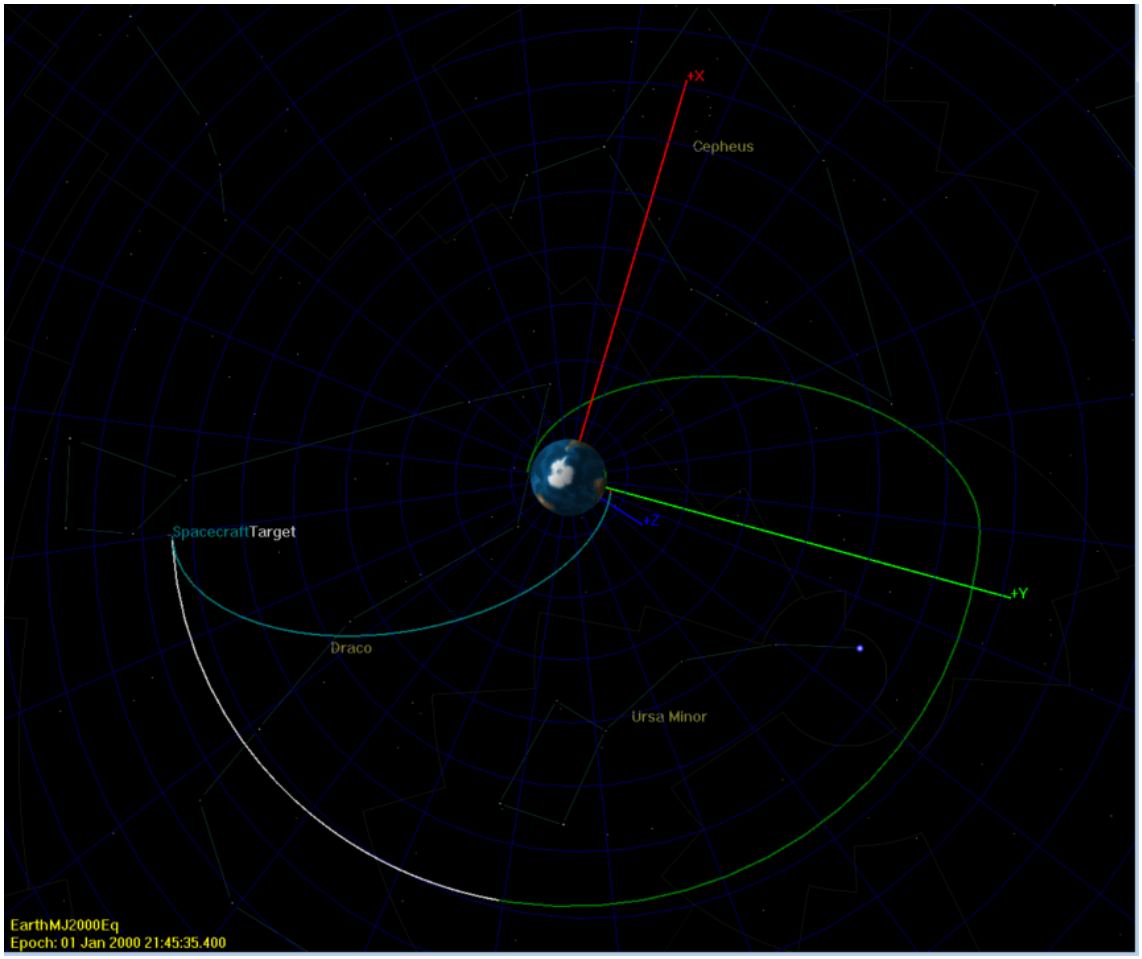

Figure 7.4: Results of space rendezvous.

Figure 7.4 shows the space rendezvous trajectories, where the green orbit is the launch phase and medium Earth orbit. After twelve hours of the target being in orbit, the spacecraft begins the phasing phase and then the close-range rendezvous, the blue orbit. When the spacecraft has the same position and velocity the final approaching phase is completed and the simulation is finished. Note that the white orbit is the target's orbit when the target begins the phasing phase.

Constraints	Desired	Achieved	Difference
(==) Spacecraft.EarthMJ2000Eq.X	-27678.41783200478	-27678.34369239526	0.07413960951816989
(==) Spacecraft.EarthMJ2000Eq.Y	-59649.01239181431	-59649.04903662425	-0.03664480993757024
(==) Spacecraft.EarthMJ2000Eq.Z	-13121.66365691626	-13121.65492115724	0.008735759021874401
(==) Spacecraft.EarthMJ2000Eq.VX	2.177108046251254	2.177109293086405	1.246835151569314e-06
(==) Spacecraft.EarthMJ2000Eq.VY	-1.066923377159156	-1.066920690334026	2.686825130604476e-06
(==) Spacecraft.EarthMJ2000Eq.VZ	0.2577661552825617	0.2577667463654584	5.910828966837478e-07
CONVERGED			

Figure 7.5: Final position and velocity of both spacecrafts.

Figure 7.5 shows results of the Newton iteration method that converges after 100 iterations and the difference position and velocity between the two spacecrafts has a 0.1 tolerance.

In the following we show the positions (X,Y,Z) of the spacecraft and the target spacecraft with the Earth as the center of the coordinate system. As we can see in figures 7.6, 7.7 and 7.8 the position of both spacecrafts converge to the same location.

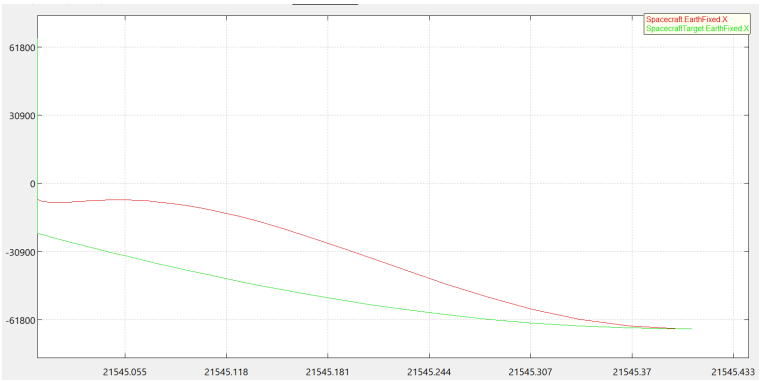

Figure 7.6: Evolution of the x coordinate position of spacecraft in red and the target spacecraft in green.

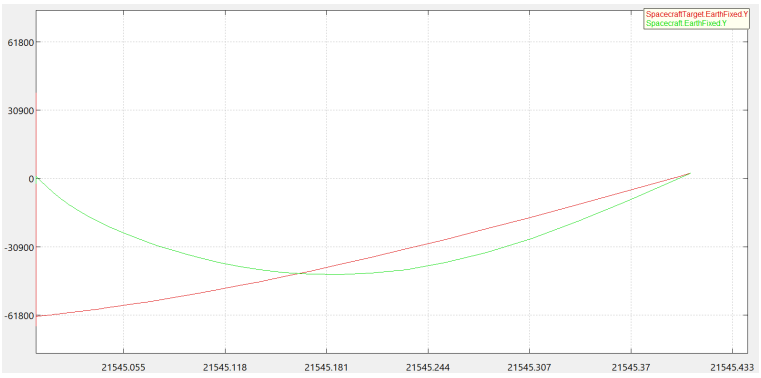

Figure 7.7: Evolution of the y coordinate position of spacecraft in green and the target spacecraft in red.

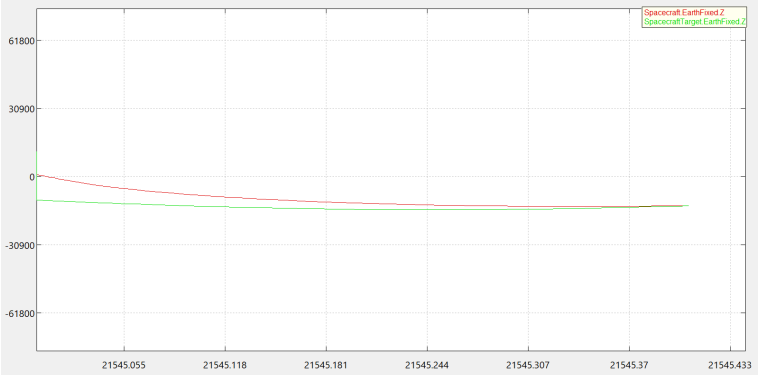

Figure 7.8: Evolution of the z coordinate position of spacecraft in red and the target spacecraft in blue.

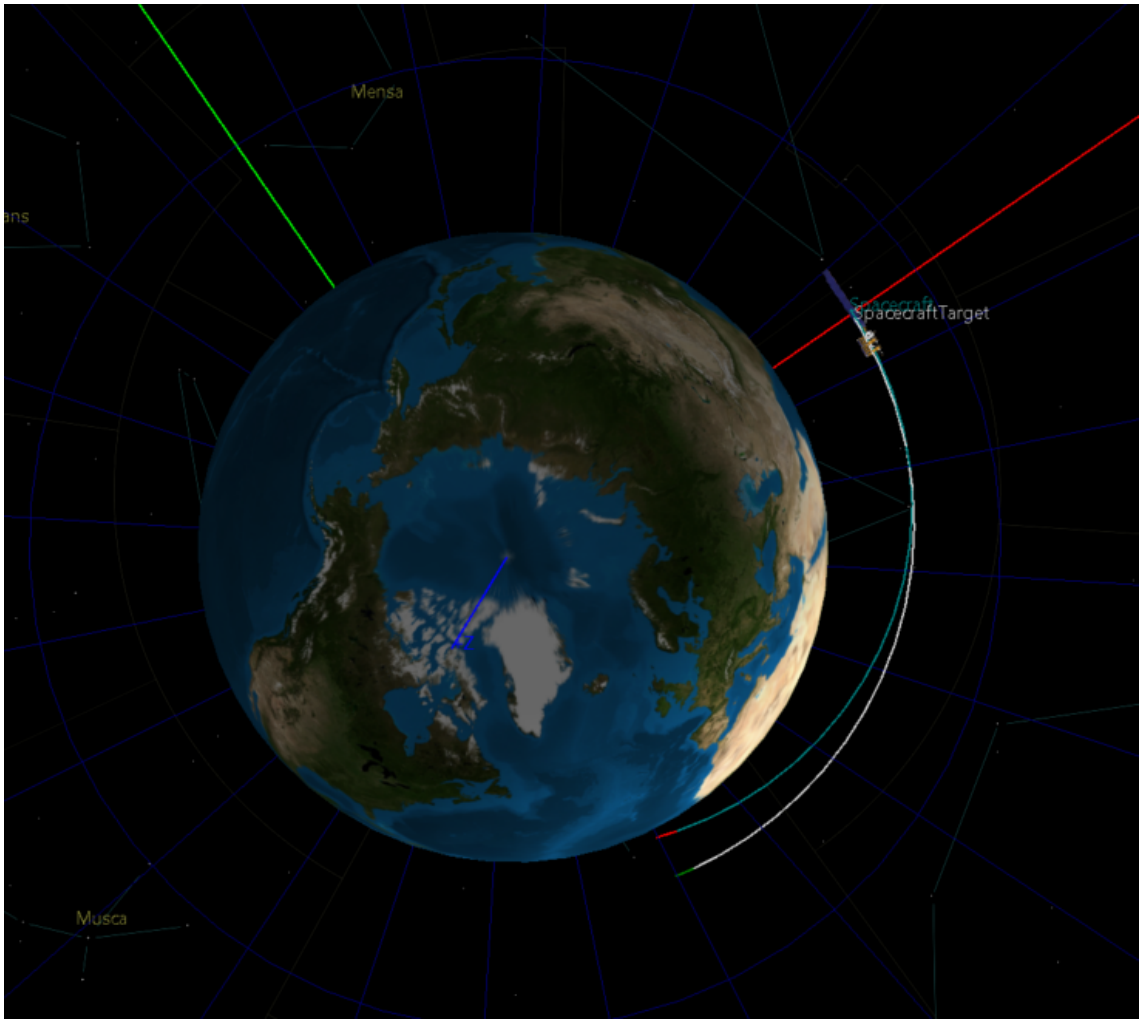

Figure 7.9: Example of burns to trajectory rendezvous.

Figure 7.9, shows a computer simulation of a finite burn of the spacecraft obtain the same orbit as the target spacecraft. In this simulation the target spacecraft had a low orbit around the Earth.

Chapter 8

Conclusions and Future Work

8.1 Conclusions

This Dissertation conducted a study about the motion of a spacecraft system. This study relates to orbit dynamics, the estimation and control of the dynamics and attitude of a satellite. A complementary problem addressed was the studied of the rendezvous orbital dynamics and control.

The chapter of orbital dynamics was concerned with the three Kepler's Laws and the Newton's Universal Law of Gravitation. Also, the relation and differences between them were analyzed. The results demonstrates that the distance between the spacecraft and the Earth's center with the Newton's Laws takes into account the forces applied to the satellite and the spacecraft dynamics, which is more precise assuming that all parameters and external forces are know.

To solve the attitude estimation of a spacecraft we used the extended Kalman filter because the spacecraft system is a nonlinear system. Chapter 5 describes the advantages and disadvantages of three different representations of spacecraft attitude. To achieve the desired attitude, the controller needs to conveniently activate the actuators. The actuators to change the attitude of a spacecraft are usually the reaction wheels. The obtained results of the attitude estimation and control of a spacecraft showed good results. In particular, it could be see that the quaternions errors converge approximately to zero.

The extra problem of this study can be viewed as an integration of all the problems previously studied. The rendezvous orbital dynamics and control uses thrusters as actuators because it is needed a force with a great magnitude to control the orbit. The chapter seven shows the different phases of spacecraft rendezvous processes and the relative dynamics of two spacecrafts. Note that the origin of coordinate system changes with the distance between the two spacecrafts as well as relative dynamics equations of the spacecraft. For the rendezvous navigation it is needful that the spacecraft uses the orbital maneuver to change its orbit. The results shows from the launch of the

target's spacecraft to the phasing, close-range rendezvous and final approaching phases.

8.2 Future Work

All the tools used and all the work done will allow further improvements and new features like the ones shown in the following list:

- In dynamic model, the next steps are add the atmospheric drag and solar radiation pressure as the interference.
- Add more sensors to spacecraft, such as horizon sensors, global positioning system thus to implement more characteristics to the spacecraft.
- Study the orbit estimation and control of a spacecraft.
- Add reaction wheels disturbances because the wheels are the source that contribute for attitude disturbances of a spacecraft, such as radial forces, axial forces, radial moments and axial moments.
- Add the docking phase of two spacecrafts.
- Add the thrusters in the attitude estimation and control of a spacecraft.

References

[1] NASA. Nutation and Precession, 2015. URL: https://space-geodesy.nasa.gov/multimedia/EarthOrientationAnimations/nutationAndPrecession.html.

[2] Darby Dyar. Kepler's Laws and Newton's Laws, 2010. URL: https://www.mtholyoke.edu/courses/mdyar/ast223/orbits/orb{_}lect.html.

[3] How to Calculate the Positions of the Planets: An Overview. URL: http://www.davidcolarusso.com/astro/.

[4] T. Helliwel and V. Sahakian. Chapter 6 Gravitation and Central-force motion. *Classic mechanics*, 2.

[5] ILS. Proton Launch System Mission Planner's Guide. *July*, (October), 2009.

[6] Yazhong Luo, Jin Zhang, and Guojin Tang. Survey of orbital dynamics and control of space rendezvous. *Chinese Journal of Aeronautics*, 27(1):1–11, 2014. URL: http://dx.doi.org/10.1016/j.cja.2013.07.042, doi:10.1016/j.cja.2013.07.042.

[7] JEAN-JACQUES E.; WEIPING LI SLOTINE. *Applied Nonlinear Control*. 1991.

[8] Austin H Gale and Peter W Likinsf. Spacecraft Dynamics and Control. 7(9):1049–1056, 1970. doi:10.1017/CBO9780511815652.

[9] I Cabrita Neves. DINÂMICA DOS SISTEMAS DE PARTÍCULAS E DOS CORPOS RÍGIDOS. 2005.

[10] James R. Wertz. Magnetic Field Models, 1978.

[11] Davide Conte and David B. Spencer. Targeting the martian moons via direct insertion into mars-orbit. *Advances in the Astronautical Sciences*, 156(August 2015):2389–2406, 2016.

[12] F Landis Markley and John L Crassidis. *Fundamentals of Spacecraft Attitude Determination and Control*, volume 2. 2013. doi:10.1007/978-1-4939-0802-8.

[13] John L. Crassidis and John L. Junkins. *Optimal Estimation of Dynamic Systems*. 2011. arXiv:arXiv:1011.1669v3, doi:10.1017/CBO9781107415324.004.

[14] P. Romero, B. Pablos, and G. Barderas. Analysis of orbit determination from Earth-based tracking for relay satellites in a perturbed areostationary orbit. *Acta Astronautica*, 136(March):434–442, 2017. URL: http://dx.doi.org/10.1016/j.actaastro.2017.04.002, doi:10.1016/j.actaastro.2017.04.002.

[15] Xichun Li, Abudulla Gani, Rosli Salleh, and Omar Zakaria. The Future of Mobile Wireless Communication Networks. *2009 International Conference on Communication Software and Networks*, pages 554–557, 2009. URL: http://ieeexplore.ieee.org/document/5076913/, doi:10.1109/ICCSN.2009.105.

[16] Christophe Bonnal, Jean Marc Ruault, and Marie Christine Desjean. Active debris removal: Recent progress and current trends. *Acta Astronautica*, 85:51–60, 2013. URL: http://dx.doi.org/10.1016/j.actaastro.2012.11.009, doi:10.1016/j.actaastro.2012.11.009.

[17] Heike Benninghoff, Florian Rems, and Toralf Boge. Development and hardware-in-the-loop test of a guidance, navigation and control system for on-orbit servicing. *Acta Astronautica*, 102:67–80, 2014. URL: http://dx.doi.org/10.1016/j.actaastro.2014.05.023, doi:10.1016/j.actaastro.2014.05.023.

[18] Wenfu Xu, Bin Liang, and Yangsheng Xu. Survey of modeling, planning, and ground verification of space robotic systems. *Acta Astronautica*, 68(11-12):1629–1649, 2011. URL: http://dx.doi.org/10.1016/j.actaastro.2010.12.004, doi:10.1016/j.actaastro.2010.12.004.

[19] Marco M. Castronuovon. Active space debris removal-A preliminary mission analysis and design. *Acta Astronautica*, 69(9-10):848–859, 2011. URL: http://dx.doi.org/10.1016/j.actaastro.2011.04.017, doi:10.1016/j.actaastro.2011.04.017.

[20] Shin Ichiro Nishida, Satomi Kawamoto, Yasushi Okawa, Fuyuto Terui, and Shoji Kitamura. Space debris removal system using a small satellite. *Acta Astronautica*, 65(1-2):95–102, 2009. doi:10.1016/j.actaastro.2009.01.041.

[21] J. C. Liou, N. L. Johnson, and N. M. Hill. Controlling the growth of future LEO debris populations with active debris removal. *Acta Astronautica*, 66(5-6):648–653, 2010. URL: http://dx.doi.org/10.1016/j.actaastro.2009.08.005, doi:10.1016/j.actaastro.2009.08.005.

[22] Hongbo Zhang and Bin Li. Velocity-to-Be-Gained Deorbit Guidance Law Using State Space Perturbation Method. 31(2009), 2018. doi:10.1061/(ASCE)AS.1943-5525.0000808.

[23] Wojciech Gołębiowski, Rafał Michalczyk, Michał Dyrek, Umberto Battista, and Kjetil Wormnes. Validated simulator for space debris removal with nets and other flexible tethers applications. *Acta Astronautica*, 129(January):229–240, 2016. doi:10.1016/j.actaastro.2016.08.037.

[24] Chaim Gartenberg. What is 5G? URL: https://www.theverge.com/2017/2/24/14701430/5g-network-explained-mobile-data-cellular-millimeter-wave.

[25] J. C. Liou and Nicholas L. Johnson. A sensitivity study of the effectiveness of active debris removal in LEO. *Acta Astronautica*, 64(2-3):236–243, 2009. doi:10.1016/j.actaastro.2008.07.009.

[26] Robin Biesbroek, Tiago Soares, Jakob Hüsing, Kjetil Wormnes, and Luisa Innocenti. The E. Deorbit CDF study: A design study for the safe removal of a large space debris. *6th The International Association for Advancement of Space Safety Conference, Montreal, Canada*, 3(April):2294–2301, 2013.

[27] Francesco Guidolin, Maziar Nekovee, Leonardo Badia, and Michele Zorzi. A cooperative scheduling algorithm for the coexistence of fixed satellite services and 5G cellular network. *IEEE International Conference on Communications*, 2015-Septe:1322–1327, 2015. doi:10.1109/ICC.2015.7248506.

[28] Barry G. Evans. The role of satellites in 5G. *2014 7th Advanced Satellite Multimedia Systems Conference and the 13th Signal Processing for Space Communications Workshop, ASMS/SPSC 2014*, 2014-Janua:197–202, 2014. doi:10.1109/ASMS-SPSC.2014.6934544.

[29] Wolfgang Rackl, Marco De Stefano, Roberto Lampariello, Nuno Santos, Pedro Serra, Marco Canetri, Finn Ankersen, and Jesus Gil-fernandez. GNC architecture for the e . Deorbit mission. 2017. doi:10.13009/EUCASS2017-317.

[30] Yiwei Liu, Alessandro Neri, Agostino Ruggeri, Anna Maria Vegni, and Senior Member. A MPTCP-Based Network Architecture for Intelligent Train Control and Traffic Management Operations. 18(9):1–13, 2016. doi:10.1109/TITS.2016.2633531.

[31] II George W. Collins. Coordinate Systems and Coordinate Transformations. In *The Foundations of Celestial Mechanics*, pages 15–38. 2004. URL: http://ads.harvard.edu/books/1989fcm..book/Chapter2.pdf.

[32] M. Catherine White. National Aeronautics and Space Administration. *Eos, Transactions American Geophysical Union*, 75(7):74, 1994. URL: http://doi.wiley.com/10.1029/94EO00779, doi:10.1029/94EO00779.

[33] Mohammed Chessab Mahdi. Orbit Design and Simulation for Kufasat Nanosatellite. *Artificial Satellites*, 50(4):157–168, 2015. doi:10.1515/arsa-2015-0013.

[34] 220 5 Orbit and Ground Track of a Satellite. *Orbit An International Journal On Orbital Disorders And Facial Reconstructive Surgery*, 1530:220–220, 2001.

[35] A.G Fallis. Orbital Mechanics for Engineering Students. *Journal of Chemical Information and Modeling*, 53(9):1689–1699, 2013. arXiv:arXiv:1011.1669v3, doi:10.1017/CBO9781107415324.004.

[36] Marius Corici, Adam Kapovits, Stefan Covaci, Alexander Geurtz, Ilie-Daniel Gheorghe Pop, and Björn Riemer. Assessing satellite-terrestrial integration opportunities in the 5G environment. 2016.

[37] ESA. Satellite for 5G, 2017. URL: http://www.esa.int/Our{_}Activities/Telecommunications{_}Integrated{_}Applications/Satellite{_}for{_}5G.

[38] Orbital Mechanics. Section 2 . Satellite Orbits. 2005:174–192, 2005.

[39] ESA. SATELLITE FOR 5G OVERVIEW. URL: https://artes.esa.int/satellite-5g/overview.

[40] ESA. CleanSat, 2016.

[41] Wikipedia. Ground station, 2018. URL: https://en.wikipedia.org/wiki/Ground{_}station.

[42] Wikipedia. Star tracker, 2018. URL: https://en.wikipedia.org/wiki/Star{_}tracker.

[43] Joe Rao. Navigating by the Stars, 2008. URL: https://www.space.com/5849-navigating-stars.html.

[44] Spacetech Gmbh Immenstaad. Coarse Earth Sun Sensor Coarse Earth Sun Sensor.

[45] ESA. Reflecting on Earth's Albedo.

[46] George Lentaris, Ioannis Stratakos, Ioannis Stamoulias, Konstantinos Maragos, Dimitrios Soudris, Manolis Lourakis, Xenophon Zabulis, and David Gonzalez-Arjona. Project HIPNOS: Case Study of High Performance Avionics for Active Debris Removal in Space. *Proceedings of IEEE Computer Society Annual Symposium on VLSI, ISVLSI*, 2017-July:350–355, 2017. doi:10.1109/ISVLSI.2017.68.

[47] N H Ri, Uhjlrq Jurzlqj, Phwkrg Sdshu, Vxevwdqfh Ehfdxvh, W K H Kdyh, W K H Vdph, Exloglqj Eorfnv, Olplwhg Zkhq, Xvlqj Wkh, Shufhswxdo Rujdql, and Dwlrq Phwkrg. Jhrphwulf frqvwuxfwlrq zklfk vkrz pruh vlplodu fkdudfwhulvwlf vxfk dv wkh jud\ fkdudfwhulvwlf 7kh. 20321:3–8.

[48] Ting Sun, Fei Xing, Xiaochu Wang, Zheng You, and Daping Chu. An accuracy measurement method for star trackers based on direct astronomic observation. *Scientific Reports*, 6(February):1–10, 2016. URL: http://dx.doi.org/10.1038/srep22593, doi:10.1038/srep22593.

[49] André Balogh. in-Flight Scientific Performance of Magnetically Clean Spacecraft : Ulysses and Cluster. (May), 2012.

[50] Ronald J Boain. A-B-Cs of Sun-Synchronous Orbit Mission Design 14 AAS / AIAA Space Flight Mechanics Conference. *14th AAS/AIAA Space Flight Mechanics Conference*, pages 1–19, 2004.

[51] Karol Seweryn, Jedrzej Baran, Tomasz Barcinski, Pablo Colmenarejo, Aleksander Los, Tomasz Kowalski, Luis Mollinedo, Dario Mora, Jacek Musial, Gabriele Novelli, Jakub Oles, Katarzyna Ososinska, Pawel Pasko, Gaetano Prisco, Tomasz Rybus, Pedro Serra, Roman Wawrzaszek, and Jesus Gil Fernandez. The prototype of space manipulator WMS LEMUR dedicated to capture tumbling satellites in on-orbit environment. *11th International Workshop on Robot Motion and Control, RoMoCo 2017 - Workshop Proceedings*, pages 15–22, 2017. doi:10.1109/RoMoCo.2017.8003887.

[52] H Laakso and T Klos. Removing strong solar array disturbances and telemetry errors from dc magnetic field measurements with a dual fluxgate technique. *2012 ESA Workshop on Aerospace EMC 2012*, (August):1–4, 2012. URL: http://www.scopus.com/inward/record.url?eid=2-s2.0-84866241821{&}partnerID=40{&}md5=cbfd79562367bbd538556005c8c2f27f.

[53] J Hoogland. Earth frozen orbits : design , injection and stability Master of Science Thesis. 2015.

[54] Gardosi Federico. *DEVELOPMENT OF A MATLAB/SIMULINK®TOOL FOR COUPLED ATTITUDE AND ORBIT CONTROL USING ELECTRIC PROPULSION FOR LOW-EARTH ORBIT SATELLITES*. PhD thesis, Politecnico di Milano.

[55] Paul Przyborski and Charles Ichoku. Three Classes of Orbit, 2009. URL: https://earthobservatory.nasa.gov/Features/OrbitsCatalog/page2.php.

[56] SpaceDataHighway Starts Full Copernicus Service, 2018. URL: https://www.gim-international.com/content/news/spacedatahighway-starts-full-copernicus-service.

[57] Land monitoring service. URL: https://land.copernicus.eu/pan-european/satellite-derived-products/eu-dem/eu-dem-v1.1.

[58] TOPEX/POSEIDON AND JASON – 25 YEARS OF HIGH PRECISION OCEAN ALTIMETRY, 2017. URL: https://www.eumetsat.int/website/home/News/DAT{_}3594994.html.

[59] Forecast of Aerosols Optical Depth. URL: http://macc.copernicus-atmosphere.eu/d/services/gac/nrt/nrt{_}opticaldepth/.

[60] Average surface air temperatures for September 2016, 2016. URL: https://climate.copernicus.eu/resources/data-analysis/average-surface-air-temperature-analysis/monthly-maps/september-2016.

[61] How the Copernicus Emergency Management Service supported responses to major earthquakes in Central Italy, 2017. URL: http://emergency.copernicus.eu/mapping/ems/how-copernicus-emergency-management-service-supported-responses-major-earth

[62] ESA. SENTINEL-6, 2015. URL: http://www.esa.int/spaceinimages/Images/2015/04/Sentinel-6.

[63] ESA. EarthCARE. URL: https://earth.esa.int/web/guest/missions/esa-future-missions/earthcare.

[64] Sun Synchronous Orbit. URL: http://tornado.sfsu.edu/geosciences/classes/m415{_}715/Monteverdi/Satellite/seasons.jpg.

[65] Earth-centered inertial. URL: https://en.wikipedia.org/wiki/Earth-centered{_}inertial.

[66] Longitude Latitude relationships. URL: https://commons.wikimedia.org/wiki/File:ECEF{_}ENU{_}Longitude{_}Latitude{_}relationships.svg.

[67] ESA. Conventions. URL: https://sentinel.esa.int/web/sentinel/user-guides/sentinel-3-altimetry/definitions/conventions.

[68] eoPortal News. STRaND-1 (Surrey Training, Research and Nanosatellite Demonstrator). URL: https://directory.eoportal.org/web/eoportal/satellite-missions/content/-/article/strand-1.

[69] ESA. Trajectory Search, 2016. URL: https://trajbrowser.arc.nasa.gov/traj{_}browser.php.

[70] ESA. Trajectory Search, 2016. URL: https://trajbrowser.arc.nasa.gov/traj{_}browser.php.

[71] ESA. Trajectory Search, 2016. URL: https://trajbrowser.arc.nasa.gov/traj{_}browser.php.

[72] ESA. EUROPE DOMINATING SATELLITE STAR-TRACKER MARKET, 2012. URL: http://www.esa.int/Our{_}Activities/Space{_}Engineering{_}Technology/Europe{_}dominating{_}satellite{_}startracker{_}market/(print).

[73] Star tracker. URL: https://en.wikipedia.org/wiki/Star{_}tracker.

[74] Earth & Space Science News. Earth's Wobbly Path Gives Clues to Its Core, 2017. URL: https://eos.org/meeting-reports/earths-wobbly-path-gives-clues-to-its-core.

[75] Chris Peat. Definition of "azimuth". URL: http://www.heavens-above.com/glossary.aspx?term=azimuth.

[76] Altitude & Azimuth: The Horizontal Coordinate System. URL: https://www.timeanddate.com/astronomy/horizontal-coordinate-system.html.

[77] ESA. Clean Space. URL: http://www.esa.int/Our{_}Activities/Space{_}Engineering{_}Technology/Clean{_}Space/Images.

[78] ESA. The clean way is the right way, 2016. URL: http://www.esa.int/Our{_}Activities/Space{_}Engineering{_}Technology/Clean{_}Space/The{_}Challenge.

[79] David Szondy. Space fishing: ESA floats plan to net space junk, 2014. URL: https://newatlas.com/esa-clean-space-junk-edeorbit/30972/.

[80] VICTOR INVESTMENTS. Global Invacom, our satellite play, 2017. URL: https://vpmsingapore.wordpress.com/2017/06/21/global-invacom-our-satellite-play/.

[81] Kepler's Laws of Planetary Motion, 2000. URL: http://www.cas.miamioh.edu/{~}marcumsd/p111/lectures/kepler.htm.

[82] Yanru Chen. Conservation of Angular Momentum and Kepler's Second Law. URL: https://eloisechen.wordpress.com/2013/02/20/conservation-of-angular-momentum-and-keplers-second-law/.

[83] David Colarusso. How to Calculate the Positions of the Planets: An Overview. URL: http://www.davidcolarusso.com/astro/{%}0A.

[84] NASA. General Mission Analysis Tool (GMAT) v.R2017a. URL: https://software.nasa.gov/software/GSC-17177-1.